INFLUENCE OF THE PRESENCE OF REPRESENTATIVE MOLECULES OF PYROLYSIS BIO-OILS ON THE HYDROTREATING OF GUAIACOL AND XYLENE OVER A NICKEL-ALUMINOSILICATE CATALYST.

RAÚL ANDRÉS REDONDO SERRANO
CHEMICAL ENGINEER

UNIVERSIDAD INDUSTRIAL DE SANTANDER
FACULTAD DE INGENERÍAS FISICOQUÍMICAS
ESCUELA DE INGENIERÍA QUÍMICA
MAESTRÍA EN INGENIERÍA QUÍMICA
BUCARAMANGA
2021

INFLUENCE OF THE PRESENCE OF REPRESENTATIVE MOLECULES OF PYROLYSIS BIO-OILS ON THE HYDROTREATING OF GUAIACOL AND XYLENE OVER A NICKEL-ALUMINOSILICATE CATALYST.

RAÚL ANDRÉS REDONDO SERRANO
CHEMICAL ENGINEER

RESEARCH WORK PRESENTED AS A REQUIREMENT TO APPLY FOR THE DEGREE OF
MAGÍSTER EN INGENIERÍA QUÍMICA

ADVISOR
Prof. VÍCTOR GABRIEL BALDOVINO MEDRANO
CHEMICAL ENGINEER, Ph. D.

CO-ADVISOR
IVÁN DARÍO MORA VERGARA
CHEMICAL ENGINEER, M.Sc.

UNIVERSIDAD INDUSTRIAL DE SANTANDER
FACULTAD DE INGENERÍAS FISICOQUÍMICAS
ESCUELA DE INGENIERÍA QUÍMICA
MAESTRÍA EN INGENIERÍA QUÍMICA
BUCARAMANGA
2021

ACKNOWLEDGMENTS

I want to thank the Industrial University of Santander, especially the School of Chemical Engineering for their valuable intellectual and economic help during my master's degree. To my director, Professor Víctor Gabriel Baldovino and my co-director Iván Mora, for their valuable teachings, good advice, great patience and effective help. In addition, I thank my fellow graduate students, undergraduate students, and other members of the Centro de Investigaciones en Catálisis (CICAT) for their collaboration and pleasant company, without their help, none of this would have been possible, thank you with all my heart.

DEDICATION

Este trabajo es dedicado a mi madre Elvia Clemencia Serrano Rincón y a mi tía Carmen Sofía Serrano Ramírez, por su incondicional cariño y ayuda.

CONTENTS

Page

INTRODUCTION 11
1. EXPERIMENTAL SECTION 18
1.1 REACTANTS. 18
1.2 SYNTHESIS OF THE CATALYST. 18
1.3 CATALYST CHARACTERIZATION. 19
1.4 CATALYTIC TESTS. 22
2. RESULTS AND DISCUSSION 26
2.1 PHYSICOCHEMICAL PROPERTIES OF THE CATALYST. 26
2.2 CATALYTIC RESULTS 29
2.2.1 Catalytic performance for the co-processing of guaiacol and xylene. 29
2.2.2 Catalytic performance in the presence of pyridine. 31
2.2.3 Catalytic performance in the presence of acetic acid. 34
2.2.4 Catalytic performance in the presence of water. 35
2.2.5 Catalytic performance in the presence of pyridine and acetic acid. 36
2.2.6 Catalytic performance in the presence of pyridine, acetic acid and water. 37
2.3 INFRARED SPECTROSCOPY ANALYSIS OF THE SPENT CATALYST. 38
2.4 GLOBAL RESULTS OF CATALYTIC ACTIVITY AND YIELD TO ISO CONVERSION OF GUAIACOL. 40
3. CONCLUSIONS 42
BIBLIOGRAFY 43
ANNEXES 49

LIST OF FIGURES

Page

Figure 1. Guaiacol hydrodeoxygenation routes. 13

Figure 2. XRD pattern of fresh catalyst Ni/Aluminosilicate. 27

Figure 3. Guaiacol and xylene conversion and yield of at 190 ºC (left) and 250 ºC (right); pH2 = 69 bar; guaiacol concentration of 0.272 M in xylene. 30

Figure 4. Conversion and yield results of guaiacol and xylene (left) and pyridine (right) at 250 ºC; pH2 = 69 bar; feed concentration: guaiacol 0.272 M and pyridine 0.182 M in xylene. 33

Figure 5. Conversion and yield results of guaiacol and xylene in presence of acetic acid at 190 ºC (left) and 250 ºC (right) ; pH2 = 69 bar; feed concentration: guaiacol 0.272 M and acetic acid 0.182 M in xylene. 35

Figure 6. Reactivity results of guaiacol and xylene in presence of water at 190ºC (left) and 250ºC (right); pH2 = 69 bar; feed concentration: guaiacol 0.272 M and water 0.182 M in xylene. 36

Figure 7. Guaiacol reactivity in the presence of pyridine and acetic acid at 250ºC; pH2 = 69 bar; feed concentration: guaiacol 0.272 M and pyridine 0.091 M and acetic acid 0.091 M in xylene (left). Conversion and yield of pyridine and acetic acid of the same test. 37

Figure 8. Infrared spectrum of the catalyst fresh and after reaction at 250ºC and 69 bar of H2 pressure with guaiacol, guaiacol+pyridine, and guaiacol+acetic acid in xylene. 39

Figure 9. Yields to iso-conversion of 10% guaiacol (a). Yields to iso-conversion of 5% guaiacol (b). 41

LIST OF TABLES

Page

Table 1. Reactivity in terms of Conversion (X) and Selectivity (S) to main products of hydrodeoxygenation of guaiacol over different heterogeneous supported metal catalysts. 14
Table 2. Summary of catalytic experiments. 23
Table 3. Scherrer equation results for NiO crystal size of fresh catalyst. 28
Table 4. Summary of textural properties of the materials before (Al_2O_3, Ni/Al_2O_3-SiO_2) and after the hydrothermal test (Al_2O_3-HT, Ni/Al_2O_3-SiO_2-HT) at 180ºC..... 29
Table 5. Results of catalytic activity for all experiments. 40

LIST OF ANNEXES

Page

ANNEX A. Preliminary tests (Pretests). 49
ANNEX B. Results of evolution of conversion and performance of Guayacol of all the tests of the model carried out. 50
ANNEX C. Results of physicochemical properties. 53
ANNEX D. Mass spectrum of Acetic Acid and Dioxane in preliminary test 2. 55

RESUMEN

TÍTULO: INFLUENCIA DE LA PRESENCIA DE MOLÉCULAS REPRESENTATIVAS DE BIOACEITES DE PIRÓLISIS EN EL HIDROTRATAMIENTO DE GUAYACOL Y XILENO SOBRE UN CATALIZADOR DE NÍQUEL-ALUMINOSILICATO.*

AUTOR: RAÚL ANDRÉS REDONDO SERRANO**

PALABRAS CLAVE: HIDRODEOXIGENACIÓN, GUAYACOL, PIRIDINA, ÁCIDO, AGUA.

DESCRIPCIÓN:

La hidrodesoxigenación catalítica (HDO) es un tratamiento que permite la producción de biocombustibles mediante la eliminación de heteroátomos de oxígeno de bioaceites de pirólisis rápida de biomasa lignocelulósica. Sin embargo, estudiar la complejidad del proceso requiere el uso de mezclas modelo que representen en gran medida la carga real para ser analizadas a mayor profundidad. El guayacol es una molécula modelo ampliamente utilizada ya que tiene dos grupos oxigenados de interés; hidroxilo (-OH) y metoxilo ($-OCH_3$), comúnmente presentes en compuestos derivados de lignina y precursores de coque durante la HDO. Además, los bioaceites contienen varios grupos moleculares orgánicos como ácidos, cetonas, fenoles, una abundante concentración de agua, y algunas trazas de grupos nitrógeno. En este sentido, se realizó un estudio sobre la influencia de la presencia de diversos tipos de moléculas representativas de bioaceites de pirólisis en el coprocesamiento de guayacol y xileno sobre un catalizador de níquel-aluminosilicato. En concreto, se analizaron tres moléculas representativas posiblemente inhibidoras: piridina, ácido acético y agua empleando pruebas catalíticas que se realizaron en un reactor discontinuo a 250 y 190ºC, presión de H_2 de 6,9 MPa, 750 rpm de agitación. Como resultado de este estudio, se encontró que en las condiciones empleadas, la piridina inhibe fuertemente al guayacol, afectando su desoxigenación y ocupando sitios metálicos y ácidos del soporte, formando piperidina. Por otro lado, el ácido acético disminuye la actividad catalítica pero no la selectividad, y en presencia de piridina reacciona para producir acetilpiperidina. El agua no afectó significativamente la actividad o la selectividad.

---

* *Proyecto de Maestría.*

** *Facultad de Ingenierías Fisicoquímicas. Escuela de Ingeniería Química. Director: Víctor Gabriel Baldovino Medrano, Ingeniero Químico, Ph. D. Codirector: Iván Darío Mora Vergara, Ingeniero Químico, M. Sc*

ABSTRACT

TITTLE: INFLUENCE OF THE PRESENCE OF REPRESENTATIVE MOLECULES OF PYROLYSIS BIO-OILS ON THE HYDROTREATING OF GUAIACOL AND XYLENE OVER A NICKEL-ALUMINOSILICATE CATALYST.[†]

AUTHOR: RAÚL ANDRÉS REDONDO SERRANO[**]

KEYWORDS: HYDRODEOXYGENATION, GUAIACOL, PYRIDINE, ACID, WATER.

DESCRIPTION:

Catalytic hydrodeoxygenation (HDO) is a treatment that allows the production of biofuels by removing oxygen heteroatoms from bio-oils obtained from the rapid pyrolysis of lignocellulosic biomass. However, studying the complexity of the process requires the use of model mixtures that represent the real reactor feed in a certain way to be analyzed in greater depth. Guaiacol is a model molecule widely used in numerous catalytic studies since it has two oxygenated groups of interest; hydroxyl (-OH) and methoxyl ($-OCH_3$), commonly present in compounds derived from lignin and coke precursors during HDO. Also, bio-oils have the presence of several organic molecular groups such as acids, ketones, phenols, an abundant concentration of water, and some traces of nitrogen groups. In this sense, a study was carried out on the influence of the presence of various types of representative molecules of pyrolysis bio-oils on the co-processing of guaiacol and xylene over a nickel-aluminosilicate catalyst. Specifically, three representative possibly inhibitory molecules were analyzed: pyridine, acetic acid, and water employing catalytic tests that were carried out in a batch reactor at 250 and 190ºC, H_2 pressure of 6.9 MPa, 750 rpm of stirring. As a result of this study, it was found that under the conditions used, pyridine strongly inhibits guaiacol, affecting its deoxygenation and occupying metallic and acid sites of the support, forming piperidine. On the other hand, acetic acid decreases the catalytic activity but not selectivity, and in the presence of pyridine reacts to produce acetylpiperidine. Water didn't significantly affect activity or selectivity.

[†] *Magister Project*

[**] *Facultad de Ingenierías Físicoquímicas. Escuela de Ingeniería Química. Advisor:: Víctor Gabriel Baldovino Medrano, Chemical Engineer, Ph. D. Co-advisor: Iván Darío Mora Vergara, Chemical Engineer, M. Sc*

INTRODUCTION

Lignocellulosic biomass can be converted into a biofuel through a rapid pyrolysis route. Pyrolysis is made by rapidly heating biomass to ~500ºC in a short residence time (~ 1 s) and under an oxygen-free atmosphere. A dark liquid product called bio-oil is thus produced. Bio-oils require refinement to lower their acidity, viscosity, and enhancing their heating capacity and thermal stability [1]. These properties are a function of its high oxygen content; indeed, bio-oils main contain up to 300 oxygenated compounds which constitute between 35 and 40% of their composition, depending on the biomass source and pyrolysis conditions [2]–[5].

Hydrotreating is the industrial process for refining fuels by the hydrogen mediated removal of heteroatoms such as metals, e.g. nickel and vanadium, (hydrodemetalation), sulfur (hydrodesulfurization), nitrogen (hydrodenitrogenation), and oxygen (hydrodeoxygenation). Furthermore, hydrotreating converts aromatics (hydrodearomatization) into saturated hydrocarbons whose properties are most desirable in fuels. In this sense, this type of process has been applied to refine crude bio-oils, specifically the hydrodeoxygenation process (HDO), since by eliminating the oxygen heteroatoms present in the bio-oils it is possible to obtain fuels similar to the conventional ones, increasing their calorific value and stability [1], [6].

One of the first works on the hydrodeoxygenation of biooils was done by Elliot and Baker [7]. They used NiMo and CoMo catalysts supported on alumina in the

[1] H. Wang, J. Male, and Y. Wang. ACS Catal. (2013) vol. 3, no. 5, pp. 1047–1070.
[2] T. Cheng, Y. Han, Y. Zhang, and C. Xu. Fuel. (2016) vol. 172, pp. 49–57.
[3] Y. Liu et al. Energy and Fuels. (2012) vol. 26, no. 7, pp. 4532–4539.
[4] R. J. Evans and T. a Milne. Energy & Fuels. (1987) vol. 1, no. 2, pp. 123–138.
[5] J. L. Chukwuneke et al. Heliyon. (2019) vol. 5, no. 6, pp. 1–7, 2019.
[6] M. Lu et al. Ind. Eng. Chem. Res.(2019) vol. 58, no. 4, pp. 1513–1524.
[7] D. C. Elliott and E. G. Baker. United States. Dept. Energy. Off. Sci. Tech. Information.(1968) no. 1, pp. 1–64.

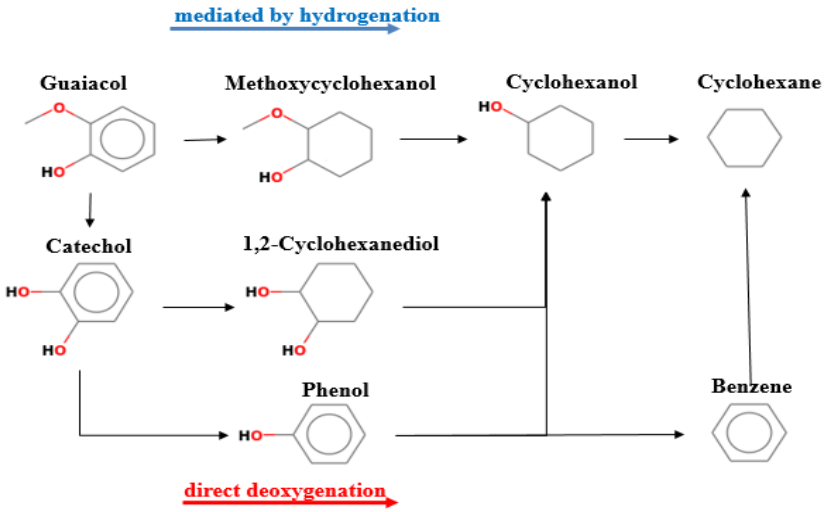
continuous hydrotreating of a bio-oil. These catalysts were active in the reaction but after several hours of operation, plugging was evidenced due to the formation of coke when operating temperatures higher than 300ºC. Hence, it was necesary that the HDO process for bio-oils should be carried out in two stages. The first stage consists of a moderate hydrotreatment at temperatures below 280ºC in order to stabilize the most reactive molecules of the bio-oil, such as methoxyphenols and biphenols. The second stage is carried out at temperatures above 300ºC and in it phenol-type molecules are transformed into hydrocarbons with a higher calorific value through complete deoxygenation [8]. This work focuses on the first stage.

2-Methoxyphenol (guaiacol) is often used as a model compound for studying the reactivity of potential catalysts for the hydrodeoxygenation of bio-oils at laboratory scale [6], [9]–[11]. The interest in guaiacol lies in the fact that this molecule has two functional groups; *hydroxyl* (R-OH) and *methoxy* (RO-CH_3), common in bio-oils. These bonds represent derived phenolic monomers from lignocellulosic biomass with a tendency to form high molecular weight compounds that deactivate the catalyst during hydrotreatment [6], [8]. The reaction routes that guaiacol typically follow to achieve its hydrodeoxygenation are found in figure 1 [9], [12]. Two main reaction routes are depicted; one where the initial demethylation of the methoxy group of the compound further leads to direct deoxygenation and another where deoxygenation is preceded by the hydrogenation of the aromatic ring of the molecule. The problem with the first route is that the formation of catechol by demethylation produces a methyl radical (CH_3·) that may lead to the formation of heavy molecular weight compounds through undesired methyl substitution reactions

[6] M. Lu et al. Ind. Eng. Chem. Res.(2019) vol. 58, no. 4, pp. 1513–1524.
[8] E. Laurent, A. Centeno, and B. Delmon. Stud. Surf. Sci. Catal.(1994) vol. 88, no. C, pp. 573–578.
[9] I. D. Mora-Vergara et al. Catal. Today. (2018) vol. 302, pp. 125–135.
[10] I. D. Mora-Vergara et al. Appl. Catal. A Gen.(2014) vol. 474, pp. 59–68.
[11] A. N. Kay Lup et al. J. Ind. Eng. Chem. (2017) vol. 56, pp. 1–34.
[12] W. Song et al. Green Chem.(2015) vol. 17, no. 2, pp. 1204–1218.

favored by the acidity of the support. This kind of compounds tend to deactivate the catalyst [8], [13]. In the case of the reaction route mediated by hydrogenation, the methanol and the water produced are rather desirable despite the fact that a larger consumption of H_2 is required. While the direct deoxygenation route generally is generally favored over transition metals such as Co, Mo and Fe [14]–[16], the route mediated by hydrogenation is catalyzed by highly hydrogenating metals such as Ni, Pd, and Pt, see table 1 for details [17]–[19].

Figure 1. Guaiacol hydrodeoxygenation routes.



[8] E. Laurent, A. Centeno, and B. Delmon. Stud. Surf. Sci. Catal.(1994) vol. 88, no. C, pp. 573–578.
[13] E. Laurent and B. Delmon. Appl. Catal. A, Gen. (1994) vol. 109, no. 1, pp. 77–96, 1994.
[14] T. Mochizuki et al. Appl. Catal. B Environ. (2014) vol. 146, pp. 237–243.
[15] V. N. Bui et al. Appl. Catal. B Environ. (201) vol. 101, no. 3–4, pp. 239–245.
[16] C. Li et al. ACS Catal.(2020) pp. 14624–14639.
[17] M. V. Bykova et al. Catal. Today (2014) vol. 220–222, pp. 21–31.
[18] Y. K. Hong et al. Appl. Catal. B Environ. (2014) vol. 150–151, pp. 438–445.
[19] M. Hellinger et al. Appl. Catal. A Gen. (2015) vol. 490, pp. 181–192.

Table 1. Reactivity in terms of Conversion (X) and Selectivity (S) to main products of hydrodeoxygenation of guaiacol over different heterogeneous supported metal catalysts.

Metal Catalyst	Main Product	Type	T (K)	P (bar)	X (%)	S (%)	Reaction Time (h)	Ref
Pt/H-MFI-90(1.0 wt% Pt)	Cyclohexane	Batch	453	50	100	93	5	[19]
NiCu/SiO_2-ZrO_2 (52 wt% Ni, 5.6 wt% Cu)	Cyclohexane	Batch	593	170	95	67	1	[17]
Pd/WOx/Al_2O_3 (2.0 wt% Pd, 32 wt% W)	Cyclohexane	Batch	573	70	100	88	2.5	[18]
Co/SiO_2 (20 wt% Co)	Benzene	Batch	573	10	100	53.1	1	[14]
ReOx/SiO_2	Cyclohexane	Batch	573	50	81	54.3	4.2	[20]
Fe/CeO_2 (3 wt% Fe)	Phenol	Continuous	673	1.01	100	57	-	[16]
Sn/Inconel monolith (8.01 wt% Sn)	Phenol	Continuous	673	1.01	10	90	-	[21]
Rh/C (5.0 wt% Rh)	Phenol	Batch	523	40	65	36	2	[22]

Although conventional crude hydrotreating catalysts were first used for the hydrodeoxygenation of model mixtures of bio-oils, these catalysts present several shortcomings [9], [13], [15], [23]. First, these catalysts based on sulfides, typically

[9] I. D. Mora-Vergara et al. Catal. Today. (2018) vol. 302, pp. 125–135.
[13] E. Laurent and B. Delmon. Appl. Catal. A, Gen. (1994) vol. 109, no. 1, pp. 77–96, 1994.
[14] T. Mochizuki et al. Appl. Catal. B Environ. (2014) vol. 146, pp. 237–243.
[15] V. N. Bui et al. Appl. Catal. B Environ. (201) vol. 101, no. 3–4, pp. 239–245.
[16] C. Li et al. ACS Catal.(2020) pp. 14624–14639.
[17] M. V. Bykova et al. Catal. Today (2014) vol. 220–222, pp. 21–31.
[18] Y. K. Hong et al. Appl. Catal. B Environ. (2014) vol. 150–151, pp. 438–445.
[19] M. Hellinger et al. Appl. Catal. A Gen. (2015) vol. 490, pp. 181–192.
[20] K. Leiva et al. Appl. Catal. A Gen. (2015) vol. 505, pp. 302–308.
[21] M. Á. González-Borja and D. E. Resasco. Energy and Fuels. (2011) vol. 25, no. 9, pp. 4155–4162.
[22] W. Mu et al. Bioresour. Technol. (2014) vol. 173, pp. 6–10.
[23] A. Gutierrez et al. Catal. Today. (2017) vol. 285, pp. 125–134.

Co-MoS_2/Al_2O_3 and Ni-MoS_2/Al_2O_3, are poorly efficient in the remotion of oxygen heteroatoms during co-processing of bio-oils in hydrotreating reactors [24]. Also they prone to deactivation by coking during operation [8], [9]. Also, they require the presence of sulfur in the reaction atmosphere for maintaining the active sites of the MoS_2 phase [15]. Furthermore, bio-oils usually have next to no sulfur contents (< 0.06 wt. %) thus a hydrodeoxygenation process based on conventional catalysts would require the addition of an external sulfur source which is undesirable both from the economic and environmental standing points [5]. This makes supported metallic candidates interesting for hydrodeoxygenation processes, particularly when considering the co-processing of conventional fuels such as diesel and bio-oils in a reactor placed at the exit of a hydrotreating unit, since these materials do not require sulfur for its activity [24], [25].

The co-processing of bio-oils and crude oil in an existing refinery is an alternative to reduce investment and production prices of biofuels by using the existing infrastructures, as well as the distribution system can also be used to distribute biofuels [25], [26]. Therefore, it is interesting to consider the addition of a reactor devoted to the simultaneous hydrodearomatization of an already refined diesel cut and to the hydrodeoxygenation of the bio-oils using a catalyst that does not require sulfur for its operation. In this sense, the formulation of a supported metallic catalyst for this reactor must balance a hydrogenating capacity, activating the hydrogen on the surface of the metal, with the acidity of the support, participating in the activation

[5] J. L. Chukwuneke et al. Heliyon. (2019) vol. 5, no. 6, pp. 1–7, 2019.
[8] E. Laurent, A. Centeno, and B. Delmon. Stud. Surf. Sci. Catal.(1994) vol. 88, no. C, pp. 573–578.
[9] I. D. Mora-Vergara et al. Catal. Today. (2018) vol. 302, pp. 125–135.
[15] V. N. Bui et al. Appl. Catal. B Environ. (201) vol. 101, no. 3–4, pp. 239–245.
[24] C. M. Celis-Cornejo et al. Energy and Fuels. (2018) vol. 32, no. 8, pp. 8715–8726.
[25] S. Bezergianni et al. Prog. Energy Combust. Sci. (2018) vol. 68, pp. 29–64.
[26] A. T. Espinoza Pérez et al. Renew. Sustain. Energy Rev.(2017) vol. 69, pp. 350–359.

and breaking of CO bonds, to provide the material with a well-balanced bifunctionality [12], [27]–[30].

We have shown that a well-balanced monometallic Ni/aluminosilicate formulation can be highly effective for the hydrodeoxygenation of guaiacol in the presence of xylene [31]. Thermodynamic analysis of the guaiacol hydrodeoxygenation reaction routes using this material was performed, finding that the most favored route was the one mediated by hydrogenation [32]. In addition, different metal loadings of this catalyst were explored, establishing optimal metal content and reaction conditions free of mass and heat transfer limitations [33]. Subsequently, a kinetic analysis of the HDO of guaiacol was carried out using Langmuir-hinshelwood modeling whose calculated parameters have thermodynamic consistency [34].

For this work, we investigated the influence of the presence of various types of representative molecules of pyrolysis bio-oils on the hydrotreating of guaiacol and xylene using this catalyst. Specifically, we selected three representative molecules found in bio-oils; namely, pyridine, acetic acid, and water. As far as the literature consulted for this work goes, the reactivity of reaction mixtures such as the ones considered herein have not been explored previously despite the large number of research papers devoted to the study of catalysts for the hydrodeoxygenation of bio-oils. The analysis of the effect that these representative bio-oil molecules may have on the HDO of guaiacol using a nickel-aluminosilicate catalyst and its physicochemical state will allow clarifying the vision on the complex mixture of

[12] W. Song et al. Green Chem.(2015) vol. 17, no. 2, pp. 1204–1218.
[27] F. Broglia et al. Fuel. (2019) vol. 243, pp. 501–508.
[28] A. J. R. Hensley et al. ACS Catal. (2018) vol. 8, no. 3, pp. 2200–2208.
[29] K. A. Goulas et al. Nat. Catal. (2019) vol. 2, no. 3, pp. 269–276.
[30] A. M. Robinson, J. E. Hensley, and J. Will Medlin. ACS Catal. (2016) vol. 6, no. 8, pp. 5026–5043.
[31] R. Redondo. Trabajo de grado Ingeniería Química. Universidad Industrial de Santander, 2017.
[32] D. Molina and P. Suárez. Trabajo de grado Ingeniería Química. Universidad Industrial de Santander, 2018.
[33] L. Restrepo and Y. Portilla. Trabajo de grado Ingeniería Química. Universidad Industrial de Santander, 2019.
[34] S. Artunduaga and C. Peralta. Trabajo de grado Ingeniería Química. Universidad Industrial de Santander, 2020.

compounds that make up a real bio-oil where some molecular families could act as potential inhibitors by compromising the integrity of the catalyst by altering its activity and/or selectivity.

1. EXPERIMENTAL SECTION

1.1 REACTANTS.

The reactants used in this research were: tetraethyl orthosilicate (Sigma-Aldrich, 98%), γ-alumina (Procatalyse), ethanol (Merck, absolute for analysis), nickel (II) nitrate (Merck, 99%), ammonia solution (Merk, 29%), guaiacol (Sigma-Aldrich, 99%), dodecane (Sigma-Aldrich, 99%), xylene "mixture of isomers" (JT Baker, 98.5%), pyridine (Sigma-Aldrich, 99%), except for acetic acid (Merk, 99%) that contained traces of dioxane according to the GC-MS results (more details in Annex D), hydrogen (99.95%, Linde), and nitrogen (99,99%, Linde). All reactants were used as received from their suppliers.

1.2 SYNTHESIS OF THE CATALYST.

The method used for synthesizing the investigated Ni/aluminosilicate catalyst consists of the impregnation of silicon over an alumina carrier; herein, a commercial γ-Al_2O_3. For this, tetraethyl orthosilicate was dissolved in ethanol and this solution was mixed with the alumina powder. Then, this mixture was rotary evaporated. The recovered solid was calcined in a tubular reactor at 480°C under an air flow of 100 mL/min. For the incorporation of nickel, a solution of an adequate concentration of nickel nitrate was contacted with the aluminosilicate at a pH ~ 12. The produced mixture was rotary evaporated, and the recovered solid was thermally treated with a similar procedure as the one used for the aluminosilicate support [31].

[31] R. Redondo. Trabajo de grado Ingeniería Química. Universidad Industrial de Santander, 2017.

1.3 CATALYST CHARACTERIZATION.

The catalyst was characterized for assessing its total nickel content, textural properties, crystallinity, the concentration of surface exposed Ni, and its acidity.

The total content of nickel in the catalyst was determined by atomic absorption using homemade calibration standards. The measurement was carried out with a Flame Atomic Absorption Agilent 240FS AA spectrophotometer. For this, a sample of ~0.5 g of the catalyst was subjected to an acid digestion process with HNO_3 (Merck, 65%) at 100°C, and further decanted and washed following the protocol presented by Uddin et al. [35].

Nitrogen adsorption-desorption isotherms were recorded to evaluate the textural properties of the materials. These measurements were made in a 3FLEX apparatus (Micromeritics). Before the analysis, the samples were degassed under vacuum at 120ºC for 2 h and 300ºC for 12 h. The specific surface area (SA_{BET}) was determined based on the theory of Brunauer, Emmett, and Teller [36] and applying the Rouquerol criterion to select the experimental points where the constant C_{BET} is minimized [37]. On the other hand, the volume and mean pore diameter of the materials was calculated using the method of Barret, Joyner, and Halenda (BHJ) [38]. For comparison purposes, the textural properties of the materials were assessed for samples of the materials after each stage of their synthesis and after performing a hydrothermal stability test. The latter was performed for the commercial γ-Al_2O_3 used in the synthesis of the catalytic material and for the finished Ni/aluminosilicate catalyst. The test consisted on taking samples of ~0.25 g of each material and putting them in a 50 ml autoclave loaded with approximately 20g of deionized type 1 water. The autoclave was then sealed and heated in a static oven

[35] A. H. Uddin et al. J. Anal. Sci. Technol. (2016) vol. 7, no. 1, pp. 1–7.
[36] S. Brunauer, P. H. Emmett, and E. Teller, J. Am. Chem. Soc. (1938) vol. 60, no. 2, pp. 309–319.
[37] F. Rodríguez-Reinoso. Stud. Surf. Sci. Catal. (2002) vol. 144, pp. 49-56.
[38] E. P. Barrett, L. G. Joyner, and P. P. Halenda. J. Am. Chem. Soc. (1951) vol. 73, no. 1, pp. 373–380.

at 180ºC for 24 h. Subsequently, it was removed from the oven and allowed to cool down to room temperature.

Crystallinity was examined with X-ray diffraction (XRD) analysis carried out with a Bruker D8 Advance diffractometer provided with a Cu Kα source operated at 40 kV and 40 mA. A sample of the catalyst was crushed in an agate mortar. It was subsequently mounted in a polymethylmethacrylate sample holder using the front fill technique. In order to obtain information on the crystallographic structure of the synthesized material the samples were scanned from 10° to 70° (2θ). Qualitative analysis of the observed peaks were carried out by comparing the pattern recorded for the catalyst with diffraction profiles reported in the PDF-2 (2019) of the ICDD database for NiO (01-075-0269) and Al_2O_3 (01-074-2206). The estimation of the average size of the crystal was obtained by the equation of Scherrer (Equation 1):

$$\beta = \frac{k\lambda}{FWHM(S)Cos\theta} \qquad \text{(Equation 1)}$$

Where, β is the crystal size (NiO particle diameter in this case), k is the crystal form factor (a constant generally equal to 1) [39] , λ is the wavelength of the radiation used (CuK α 1 = 0.15418 nm), θ is the position of the diffraction peak in radians, and FWHM(S) is the width at the mean height of the diffraction peak of the sample, calculated using the Fityk 0.9.8 software.

The concentration of surface exposed Ni was estimated by static volumetric chemisorption of H_2 at 35 °C using the same 3FLEX™ instrument mentioned before. Before testing, a sample of ca. 0.5 g was placed in a U-shaped fixed bed reactor made of quartz. The sample was reduced with hydrogen at 350 °C under a flow of 60 ml/min of H_2 for 3 h. Then, it was degassed and evacuated under vacuum until reaching the analysis temperature. The total and reversible amounts of adsorbed H_2 was obtained by extrapolating the isotherms to zero pressure. The difference between these two values results in the amount of chemisorbed H_2 from which the

[39] R. J. Farrauto and M. C. Hobson. New York: Academic Press. (2003) pp. 501–526.

number of accessible metal atoms is deduced after assuming a stoichiometric factor of 2 for Ni. The corresponding values of dispersion, metallic area, and metal particle size were calculated with expressions 2, 3, and 4, respectively:

$$D = 100\% * 100\% \frac{Q_0 S}{V_{mol} \frac{P_i}{W_i}} \quad \text{(Equation 2)}$$

$$A_{metal} = \frac{N_A Q_0 S A_{atom}}{V_{mol}} \quad \text{(Equation 3)}$$

$$d_{metal} = \frac{1000k}{\rho A_{metal}} \quad \text{(Equation 4)}$$

Where, in equation 2, D is the dispersion of Ni, Q_0 is the amount of adsorbed gas, S is the stoichiometric factor for Ni with respect to H_2, V_{mol} is the molar volume of an ideal gas at standard conditions; i.e. 22414 cm^3/mol, P_i is the fraction of the metal in the sample, and W_i is the atomic weight of the metal. In equation 3, A_{metal} is the metal area, N_A is Avogadro's number, and A_{atom} is the area of the metal atom. Finally, in equation 4, d_{metal} is the metal particle size, k is a shape factor (for these materials the particles were considered to have a spherical shape, therefore, k = 6) and ρ is the density of the metal.

The acidity of the aluminosilicate support was evaluated by studying the infrared spectrum of the adsorbed pyridine. The analysis was performed with a Nicolet iS50 spectrometer (Thermo Scientific). A previously grounded sample of the material was pressed (4.5 tons) into a wafer (20 mg, 9 mm diameter) and the wafer was placed in a homemade high-vacuum cell for analysis. The samples was first degassed under vacuum (approximately 1×10^{-6} mbar) at 500 °C for 4 h. After cooling to room temperature, a first spectrum was taken as a reference. Then, the sample was exposed to 30 mbar of pyridine for 15 min. A spectrum was recorded after degassing the sample for 1 h at 150 °C. This spectrum was taken for calculating the concentration of acid sites of the material. For this, the following equation was used:

$$Concentration\ of\ acidic\ sites = \frac{(area\ under\ the\ curve\ *\ area\ of\ wafer)}{(weight\ of\ dry\ sample\ *\ Coef\ of\ M.E.)} \quad \text{(Equation 5)}$$

Where, the area under the curve is obtained by integrating the band of interest with units of cm^{-1}, the area of the tablet in cm^2 is the area of a circle with a known radius, the weight of the dry sample in grams and the Coef of M.E. is the so-called coefficient of molar extinction. This coefficient is an empirical constant that represents the amount of energy adsorbed by an infrared beam on a material. For this case, values of 1.67 and 2.22 cm/μmol were used for the Brønsted and Lewis site bands, respectively [40].[12]

Finally, infrared spectra of the spent catalysts were also recorded after filtering the catalysts from the reaction mixture. The spectra were recorded using the attenuated total reflectance (ATR) module of the iS50 spectrometer.

1.4 CATALYTIC TESTS.

The catalytic tests were carried out following an experimental design that includes two temperature levels (190 and 250 ° C), 3 types of co-reactants (water, pyridine, and acetic acid), and 3 levels of concentration of co-reactants (0.059, 0.091, and 0.182 M) maintaining in all experiments a molar guaiacol/co-reactant ratio equal to 1.5 and a concentration of guaiacol of 0.272 M. In this sense, each reactant mixture had 0.04 moles of the given co-reactant. The experimental design was singly replicated hence making a total of 16 tests including a reference test with only guaiacol and xylene. The order of execution of the tests was randomized (see table 2).

[40] C. A. Emeis. Journal of Catalysis. (1993) vol. 141, no. 2. pp. 347–354.

Table 2. Summary of catalytic experiments.

Reaction Mixture	Temperature (°C)	Pyridine (Molarity)	Acetic acid (Molarity)	Water (Molarity)	Execution Order of the experiment
Guaiacol	250	0.000	0.000	0.000	3
Guaiacol+Water	250	0.000	0.000	0.182	9
Guaiacol +Pyridine	250	0.182	0.000	0.000	1
Guaiacol +Acid	250	0.000	0.182	0.000	2
Guaiacol +Water+Pyridine	250	0.091	0.000	0.091	7
Guaiacol +Pyridine+Acid	250	0.091	0.091	0.000	8
Guaiacol +Water+Acid	250	0.000	0.091	0.091	15
Guaiacol +Water+Pyridine+Acid	250	0.059	0.059	0.059	6
Guaiacol	190	0.000	0.000	0.000	16
Guaiacol+Water	190	0.000	0.000	0.182	4
Guaiacol +Pyridine	190	0.182	0.000	0.000	12
Guaiacol +Acid	190	0.000	0.182	0.000	5
Guaiacol +Water+Pyridine	190	0.091	0.000	0.091	14
Guaiacol +Pyridine+Acid	190	0.091	0.091	0.000	10
Guaiacol +Water+Acid	190	0.000	0.091	0.091	11
Guaiacol +Water+Pyridine+Acid	190	0.059	0.059	0.059	13

The protocol used for the catalytic tests was similar to the one described in previous works of our group [9], [10]. In general, a 500 mL stainless steel batch reactor (Parr 4570/80 series) operated at pH_2 = 6.9 MPa and stirring speed = 750 rpm was used. The reactor feed of 200 g was constant in all experiments, in the reference test was composed of 3.7 wt % guaiacol, 2 wt% dodecane which was used as an internal standard for chromatographic analysis, and 94.3 wt % xylene used as both a solvent and a model reactant for typical aromatic hydrocarbons present in diesel cuts. Before each test, the catalyst (~0.5 g) was reduced ex-situ at 350 °C for 4 h using a flow of 100 ml/min of H_2. The reactor was sealed immediately after adding the reduced catalyst to the reaction mixture. The air trapped inside the reactor was evacuated with a pressurization-depressurization cycle of N_2 (1.4 MPa) and the absence of

[9] I. D. Mora-Vergara et al. Catal. Today. (2018) vol. 302, pp. 125–135.
[10] I. D. Mora-Vergara et al. Appl. Catal. A Gen.(2014) vol. 474, pp. 59–68.

leaks was verified. Then, keeping the stirring constant, the temperature of the reactor was increased to the reaction temperature. Once this temperature was reached, the pressure of the reactor was reached by injecting H_2. During the course of the reaction, samples were taken periodically. The first sample, assigned to time zero, was taken immediately after pressurizing the reactor with H_2. Then, samples were taken at 10, 20, 30, 45, 60, 90, and 120 min. The samples of the liquid products were analyzed on an HP 6890 gas chromatograph equipped with an FID detector and an HP-1 column (100 m×0.25 mm×0.5 µm). The split-splitless inlet of the instrument was operated at 200 ºC, 2.4 bar, and 85.914 cm^3/min of He. The oven of the instrument was programmed with a temperature ramp starting at 90ºC and then increasing to 130ºC. This temperature was maintained for 0.5 min. Afterward, the temperature was increased to 180 °C and maintained therein for 0.5 min. Finally, the oven was heated to 220 ºC and kept at this temperature for 3.0 min. The heating rate used for each stage was 5 °C/min. The identification of the reaction products was carried out by comparing their retention times with those of chromatography standards and their quantification was carried out using calibration curves in order to analyze the evolution of conversion and products yields. The identification of some reaction products was also done by GC-MS analysis using an HP-1 column. After each reaction test, the final product was filtered for recovering the spent catalysts. The spent catalysts were stored in Eppendorf tubes for further ATR analysis.

The catalytic activity was expressed by the apparent initial reaction constant (k_{gua} [=] $min^{-1}g^{-1}cm^3$); assuming pseudo first-order kinetics with respect to guaiacol due to the large excess of hydrogen [9], [41]. The k_{gua} constant was calculated by linear regression of equation 6 proposed first by Gevert et al. [42].

$$-ln\left(\frac{c_i}{c_0}\right) = k_{gua} W f \left(\frac{t}{v}\right) \qquad \text{(Equation 6)}$$

[9] I. D. Mora-Vergara et al. Catal. Today. (2018) vol. 302, pp. 125–135.
[41] J. R. Restrepo-Garcia, G. E. Ramírez, and V. G. Baldovino-Medrano. Catal. Letters. (2018) vol. 148, no. 2, pp. 621–641.
[42] B. S. Gevert et al. Appl. Catal. (1987) vol. 31, no. 1, pp. 119–131.

Where, c_i and c_0 [g/ml] are the guaiacol concentration at each time t at which sample i is taken and at "time zero", respectively; W [g] is the catalyst weight and f (t/v) is the correction for volume due to samples and purges. This last term is calculated according to equation 7:

$$f\left(\frac{t}{v}\right) = \sum_{i=1}^{n} \frac{t_i - t_{i-1}}{V_{i-1}} \qquad \text{(Equation 7)}$$

Where, t_i [min] is the time elapsed until the moment when sample i is taken; $V_{(i-1)}$ [cm^3] is the volume of reaction solution that remains after taking the sample (i-1) and n is the number of samples taken. For the regression, the data obtained from the first reaction samples (from t=0 to t=30min) were taken into account since it was the initial guaiacol conversion data that fit the first-order kinetics. This procedure was also adopted for analyzing the reactivity of xylene (k_{xyl}).

The yield towards a determined product j (Y_j) was calculated by the ratio of final moles of product j over the initial moles of guaiacol.

Finally, the apparent activation energy (Ea) was estimated using the Arrhenius equation:

$$\ln(k) = -\left(\frac{E_a}{R}\right)\left(\frac{1}{T}\right) + \ln(A) \qquad (8)$$

Where, k is the apparent initial reaction constant [min^{-1}], E_a is the apparent activation energy, R is the gas constant (8.314 $J*K^{-1}*mol^{-1}$), T is the temperature in Kelvin, and A is the pre-exponential factor.

2. RESULTS AND DISCUSSION

In this section, the measured physicochemical properties of the catalyst are first presented and then its catalytic performance. The discussion is presented in different sections where the effect of each factor is explained, such as the nature of the synthetic mixture, either; acidic, nitrogenous or in the presence of water, their mixtures and a final section for the global view of the tests carried out.

2.1 PHYSICOCHEMICAL PROPERTIES OF THE CATALYST.

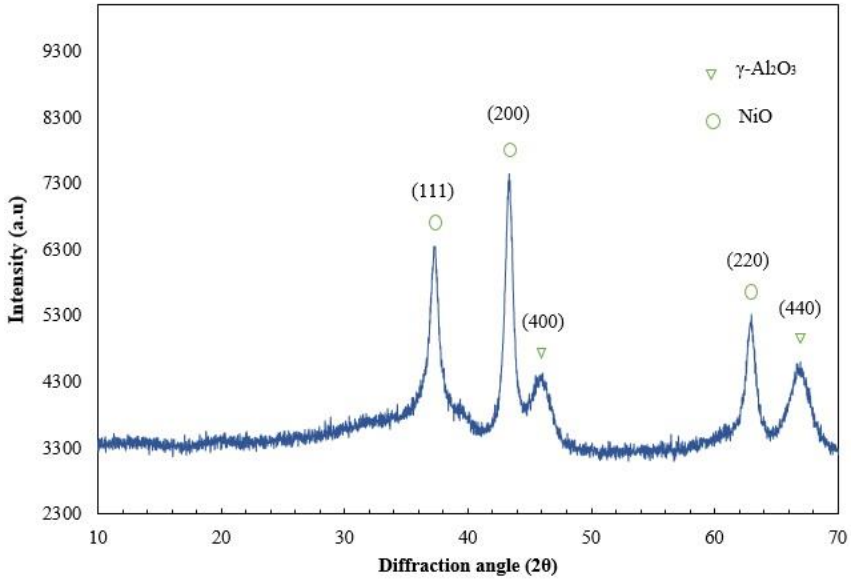
The bulk content of nickel in the catalyst was 17 wt.% according to atomic absorption results. The analysis of the static volumetric chemisorption isotherms of H_2 at 35 °C resulted in an estimation of the dispersion of Ni, Do=5.6%, thence the exposed metallic area for nickel was 5.01 m^2/g, while the average nickel metallic particle size was 23.2 nm and the molar concentration of surface-exposed nickel was 128.3 µmol Ni/g catalyst (see Annex C for the isotherms plot). For metallic catalysts, this latter amount is assumed to correspond to the concentration of active sites because, typically, the support does not catalyze the given reaction by itself. In a previous work it was shown that the conversion using only with the aluminosilicate support was negligible with respect to the final bifunctional material [31]. Considering this result, we will assume that the number of surface exposed nickel sites is an adequate metrics for the number of active sites of the catalyst. Concerning the acidity of the catalyst support, the recorded FTIR spectra for adsorbed pyridine (see Annex C for spectra plot), led to estimate a concentration of 62.0 µmol of Lewis sites and 9.3 µmol of Brønsted sites per g of support, at 150 °C. Therefore, the catalyst has a Brønsted/Lewis sites molar ratio of ~0.15 and a total acid sites of 71.3 µmol/g, which is lower than other catalyst supports in the literature [12], [43].

---

[12] W. Song et al. Green Chem.(2015) vol. 17, no. 2, pp. 1204–1218.
[31] R. Redondo. Trabajo de grado Ingeniería Química. Universidad Industrial de Santander, 2017.
[43] M. A. Ardagh et al. ACS Catal. (2016) vol. 6, no. 9, pp. 6156–6164.

Figure 2 shows the XRD pattern for a sample of the fresh catalyst. The peaks located at 2θ ~ 45.8 and 67.0° are characteristic of the crystal planes (400) and (440) of alumina, respectively.[44] In addition, the peaks appearing at 2θ ~37.1, 43.3, and 62.8 can be indexed to the (111), (200), and (220) crystal planes of NiO, respectively [45]. The absence of peaks around 2θ angles of 22° and 26.6° suggests that SiO_2 is present in an amorphous phase [46]. Table 3 presents an estimate of the average size of the NiO crystallites as from the Scherrer equation. The estimated average size of the NiO crystallites was 21.7 nm, this value is close to the determined from chemisorption, which is higher than other nickel catalysts in the literature [46], [47].

Figure 2. XRD pattern of fresh catalyst Ni/Aluminosilicate.



[44] R. M. Ravenelle et al. ACS Catal. (2011) vol. 1, no. 5, pp. 552–561.
[45] M. El-Kemary, N. Nagy, and I. El-Mehasseb, Mater. Sci. Semicond. Process. (2013) vol. 16, no. 6, pp. 1747–1752.
[46] A. R. Ardiyanti et al. Energy and Fuels. (2016) vol. 30, no. 3, pp. 1544–1554.
[47] X. Wang et al. Appl. Catal. A Gen. (2018) vol. 568, pp. 231–241.

Table 3. Scherrer equation results for NiO crystal size of fresh catalyst.

Peak	Peak máximum (rad)	FWHM	Crystallite size (nm)	Average crystallite size (nm)
111	0.325	0.009	18.6	
200	0.378	0.006	26.4	21.7
220	0.549	0.009	20.5	

The textural properties of the catalyst and the alumina are shown in table 4. The collapse of the porous structure of alumina is evidenced in terms of a detriment of the surface area and an increase in the pore diameter of this material before (Al_2O_3) and after the hydrothermal treatment (Al_2O_3-HT). On the other hand, the catalytic material used (Ni/Al_2O_3-SiO_2) retains its textural properties with slight changes. From there it was possible to establish that water under these conditions deteriorates the porous structure of the alumina, favoring the formation of boehmite and reducing its surface area. Because in these hydrodeoxygenation processes, water will always be present both at the input as an impurity of the food and the output as a reaction by-product, the catalyst must withstand environments with water at relatively high temperatures. Ravenelle et al. [44] conducted a study on the structural changes that alumina undergoes in the water at 200ºC and autogenous pressure. They found that in 10 hours the alumina was converted to hydrated boehmite (AlOOH) and this with the loss of its acid sites. Furthermore, the incorporation of a metal such as nickel or platinum to this support delayed this process by 30% that is to say at the end of 10 hours the material was 70% of being bohemite.

[44] R. M. Ravenelle et al. ACS Catal. (2011) vol. 1, no. 5, pp. 552–561.

Table 4. Summary of textural properties of the materials before (Al_2O_3, Ni/Al_2O_3-SiO_2) and after the hydrothermal test (Al_2O_3-HT, Ni/Al_2O_3-SiO_2-HT) at 180ºC.

Material	BET surface area (m^2 / g)	Pore volume (cm^3 / g)	Pore diameter (Å)
Al_2O_3	272	0.77	89
Al_2O_3-HT	51	0.32	225
Ni/Al_2O_3-SiO_2	174	0.37	67
Ni/Al_2O_3-SiO_2-HT	191	0.34	60

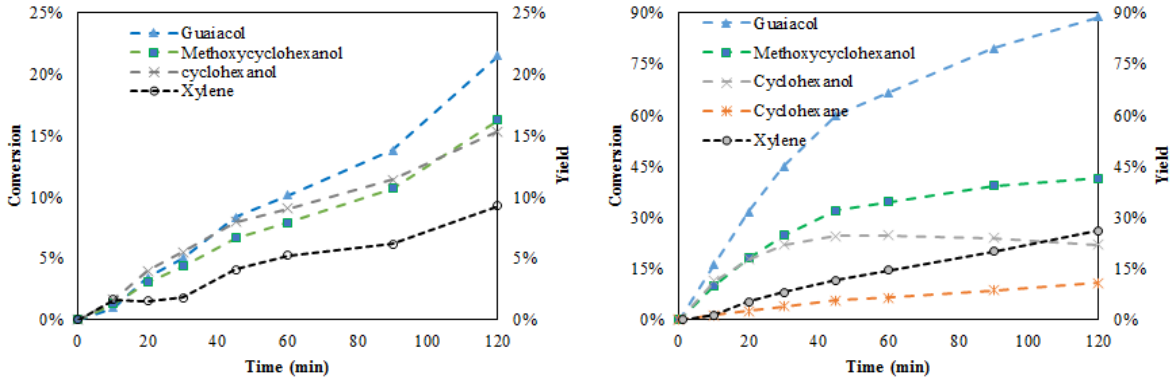
2.2 CATALYTIC RESULTS

2.2.1 Catalytic performance for the co-processing of guaiacol and xylene.

Figure 3 shows the conversion and yield for guaiacol and xylene at 190ºC and 250ºC. The conversion of guaiacol after 120 min of reaction time was ~0.21 at 190°C. Under these conditions, the reaction produced methoxycyclohexanol and cyclohexanol. In general, guaiacol followed the hydrogenation mediated route presented in figure 1 hence the molecule was first hydrogenated to form methoxycyclohexanol and then it was demethoxylated to form cyclohexanol. Therefore, the scission of the *hydroxyl* (R-OH) did not take place. At the same time, xylene reached a conversion of ~0.10 producing only dimethylcyclohexane through the hydrogenation of its aromatic ring, which is not graphed because overlaps the conversion curve. Therefore, for both guaiacol and xylene the hydrogenation of the aromatic ring is the primary step during the reaction. At 250ºC, the conversion of guaiacol was ~0.90 at 120 min hence the reaction proceeded up complete deoxygenation to form cyclohexane. In addition to this, xylene conversion reached ~0.25 and different isomers of dimethylcyclohexane were formed. The ensemble of this set of results shows that guaiacol is preferentially converted as compared to xylene over the tested catalyst. This behavior can be ascribed to the higher basicity

of guaiacol over xylene thus the adsorption of the former over the catalytic surface is preferential [48].[18]

Figure 3. Guaiacol and xylene conversion and yield of at 190 ºC (left) and 250 ºC (right); pH2 = 69 bar; guaiacol concentration of 0.272 M in xylene.



The values of the apparent pseudo-first order reaction constants for guaiacol were $k_{gua\text{-}190}$ = 0.0017 min^{-1} and $k_{gua\text{-}250}$ = 0.0188 min^{-1} indicating a one order of magnitude increase in the reaction rate when raising the temperature from 190 to 250°C. Using the above constants, the apparent activation energy for the conversion of guaiacol over the Ni/aluminosilicate catalyst was ~80 kJ / mol. This value was lower as compared to those reported by Jahromi et al. [49] over other nickel catalysts such as Ni/SiO_2-Al_2O_3 and Ni/Red Mud formulations (temperature range from 300 to 400ºC, pressure from 4.83 to 6.21 MPa, feed of 30 g of guaiacol and 4.5 g of catalyst) which were 97.5 and 90.3 kJ/mol, respectively. The guaiacol apparent activation energy for the catalyst studied herein was also lower than the 89.1 kJ/mol estimated by Bykovaa et al [50] over a more complex bimetallic mixed oxide supported

[48] A. Popov et al. J. Phys. Chem. C. (2010) vol. 114, no. 37, pp. 15661–15670.
[49] H. Jahromi and F. A. Agblevor. Appl. Catal. A Gen. (2018) vol. 558, pp. 109–121.
[50] M. V. Bykova et al. Kinet. Catal. (2013) vol. 54, no. 1, pp. 40–48.

NiCu/SiO_2–ZrO_2–La_2O_3 catalyst (temperature range from 280 to 360 ºC, feed of 33.3 g of guaiacol and a catalyst concentration in the liquid phase of 6.67 g/L). Considering that these differences are due to the nature of the catalysts that favor different reaction routes such as the dissociation of the CO bond with higher energy in the case of "NiCu" and hydrogenation of the aromatic ring in our case in particular with nickel/aluminosilicate [50]. For the hydrogenation of xylene, the apparent pseudo-first reaction rate constant also increased one order of magnitude after raising the reaction temperature from 190 to 250°C, $k_{xyl\text{-}190} = 6.34*10^{-4}$ and $k_{xyl\text{-}250} = 2.77*10^{-3}min^{-1}$, respectively. Accordingly, the reaction had an apparent activation energy of 49 kJ/mol which is within the typical value reported for the hydrogenation of other aromatics like toluene when reacted over Ni and Pt based catalysts [51], [52].

In summary, the above results show that the Ni/aluminosilicate catalyst studied herein has a very strong hydrogenation capacity which favors the aromatic ring hydrogenation mediated route of hydrodeoxygenation of guaiacol. Furthermore, guaiacol is preferentially hydrogenated over the surface of the catalyst as compared to xylene. Overall, the hydrogenation of the aromatic ring of both the tested molecules is a primary step during their transformation. Further advancement of the guaiacol reaction led to the demethoxylation producing cyclohexanol, from methoxycyclohexanol, and then it was completely deoxygenated through dehydration-hydrogenation of cyclohexanol to form cyclohexane. In contrast with xylene that was only hydrogenated without subsequent steps and no cracking products.

2.2.2 Catalytic performance in the presence of pyridine. At 190ºC, the catalyst was not active in the presence of pyridine. Therefore, pyridine was a very strong inhibiting agent for the catalyst. Figure 4 shows the results of the catalytic tests made

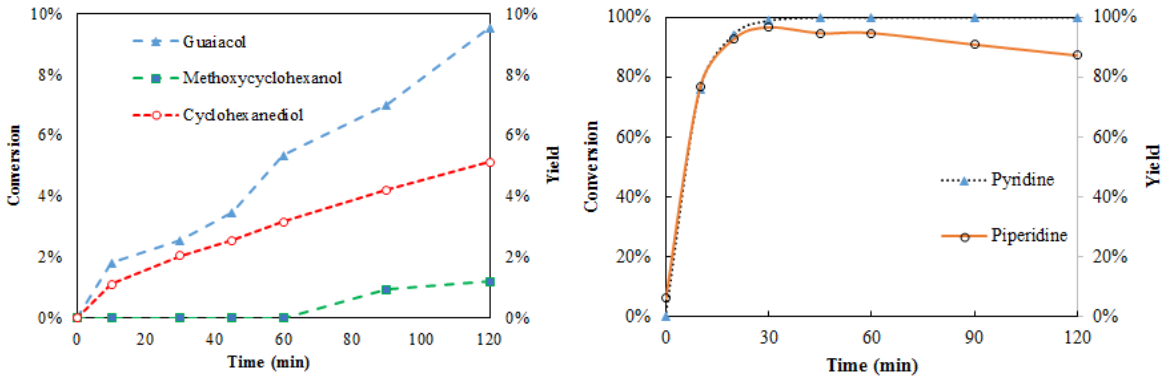
[50] M. V. Bykova et al. Kinet. Catal. (2013) vol. 54, no. 1, pp. 40–48.
[51] M. S. Lylykangas, P. A. Rautanen, and A. O. I. Krause. Ind. Eng. Chem. Res. (2002) vol. 41, no. 23, pp. 5632–5639.
[52] J. W. Thybaut, M. Saeys, and G. B. Marin. Chem. Eng. J. (2002) vol. 90, no. 1–2, pp. 117–129.

at 250ºC. At this temperature, the conversion of guaiacol reached ~0.10 after 120 min and the reaction produced cyclohexanediol first and then methoxycyclohexanol after a 60 min onset time. These results suggest that pyridine is occupying the sites that lead to breaking the CAr-O bonds of guaiacol. Therefore, it is easier to break the O-CH3, which has a lower bond dissociation energy of 57.5 kcal/mol than the CAr-OCH3, with 92.2 kcal/mol [53]. Xylene did not react during the present test confirming that pyridine was blocking its hydrogenation sites. Pyridine modifies the behavior of the catalyst since the yield is redirected towards the formation of a different product, cyclohexanediol, without the presence of deoxygenated products. This result may be related to the fact that pyridine can be chemisorbed on the acidic sites of the support (Lewis and Brønsted), which are presumed to be responsible for breaking the methoxy bond to form cyclohexanol and subsequently cyclohexane [40], [54]. This pyridine-support interaction can block the acidic sites that promote the deoxygenation pathway and follow another pathway such as the one evidenced in this case of hydrogenation and subsequent demethylation. When analyzing the reactivity of pyridine, the molecule was fully hydrogenated to piperidine in less than an hour. However, the pyridine mass balance does not agree as to the final quantity of piperidine (0.029 moles), this is lower than the stoichiometrically achieved with 100% pyridine conversion (0.033 moles). There are 0.004 moles of pyridine that are not reflected in the product, which is equivalent to 12% of the initial moles of pyridine at zero time of the reaction, showing that not all piperidine is in the liquid, therefore it could be chemisorbed on the catalyst. Also, the basicity of piperidine is greater than pyridine and should exert a stronger inhibitory effect, at least, on acidic sites. Therefore, it is possibly that both chemisorbed species exist, pyridine and piperidine blocking the sites of deoxygenation, and preventing the formation of cyclohexanol.

[40] C. A. Emeis. Journal of Catalysis. (1993) vol. 141, no. 2. pp. 347–354.
[53] A. Zheng et al. iScience. (2020) vol. 23, no. 1, pp. 1–14.
[54] J. Ryczkowski. Catal. Today. (2001) vol. 68, no. 4, pp. 263–381.

However, the doubt about which one blocks more active sites in the material may remain. In this sense, Zhao et al. [55] studied the effect of the nickel catalyst supported on alumina in the hydrogenation of pyridine to piperidine, finding that the acidic supports like Al_2O_3 promoted the adsorption of H_2 due to an electronic deficiency on the nickel surface favoring the hydrogenation of pyridine, as evidenced in this case. Furthermore, pyridine adhered more strongly to nickel than piperidine, since its chemical structure has a stronger resonance with electronegativity that compensates for the lack of electrons in nickel due to acid support, this was verified by microcalorimetric adsorption of pyridine and piperidine on the catalysts. Therefore, it is reasonable to think that pyridine is adsorbed in two sites, both in the metallic site in a planar way, decreasing the rate of hydrogenation of guaiacol, and linearly, protonating on acidic sites of the support, inhibiting the formation of cyclohexanol and redirecting the route reaction of guaiacol towards cyclohexanediol by hydrogenation-demethylation.

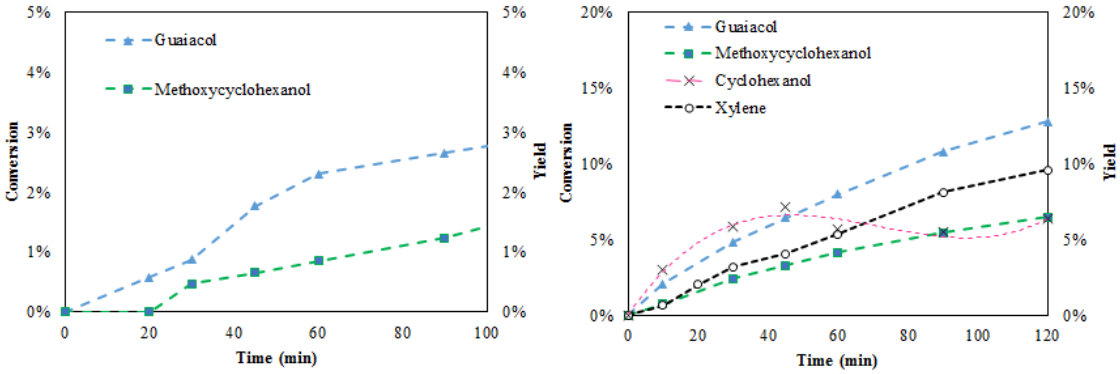
Figure 4. Conversion and yield results of guaiacol and xylene (left) and pyridine (right) at 250 ºC; pH2 = 69 bar; feed concentration: guaiacol 0.272 M and pyridine 0.182 M in xylene.



[55] J. Zhao et al. J. Phys. Chem. C. (2013) vol. 117, no. 20, pp. 10573–10580.

2.2.3 Catalytic performance in the presence of acetic acid. Figure 5 shows the reactivity results of guaiacol and xylene in the presence of acetic acid at 190ºC and 250ºC, respectively. In both cases a drop in conversion is evidenced; in particular, a loss of 18 percentage points at 190ºC and 74 percentage points at 250ºC of the final conversion with respect to the reference test. In the test at 190ºC, only 3% conversion is reached and only methoxycyclohexanol was produced. At 250°C, guaiacol follows the same reaction path that was evidenced in the reference test. In the same way, the aromatic ring of xylene was hydrogenated which contrasts with the pyridine test. This suggests that the acid is not as strong as pyridine to completely inhibit the hydrogenation of the other chemical species in the mixture and does not chemisorb on the acidic sites of the support since it allows the deoxygenation of the guaiacol. There was no conversion of acetic acid and the presence of related products in the liquid phase was not found, despite its high nominal coverage of 1122 of co-reactant moles per total moles of acid sites and 623 of co-reactant moles per total nickel exposed moles, using a relation 1:1 in both cases. A possible explanation for the poor reactivity of acetic acid is that this acid in nonpolar media, such as the one used in this test, tends to form a dimer to dissolve in non-polar solvents. The geometry that it adopts allows it to possibly be in a greater balance and therefore its reactivity decreases. So, it is possible that the acetic acid is adsorbed on the nickel decreasing the hydrogenation rates without affecting the deoxygenation. In addition to this, it is worth mentioning a preliminary test with 10 wt % of acetic acid and 3.7 wt % of guaiacol in xylene, the same behavior was observed; a minimum conversion (9%) of guaiacol without detected products and conversion of xylene or acetic acid (see Annex A).

Figure 5. Conversion and yield results of guaiacol and xylene in presence of acetic acid at 190 ºC (left) and 250 ºC (right) ; pH2 = 69 bar; feed concentration: guaiacol 0.272 M and acetic acid 0.182 M in xylene.



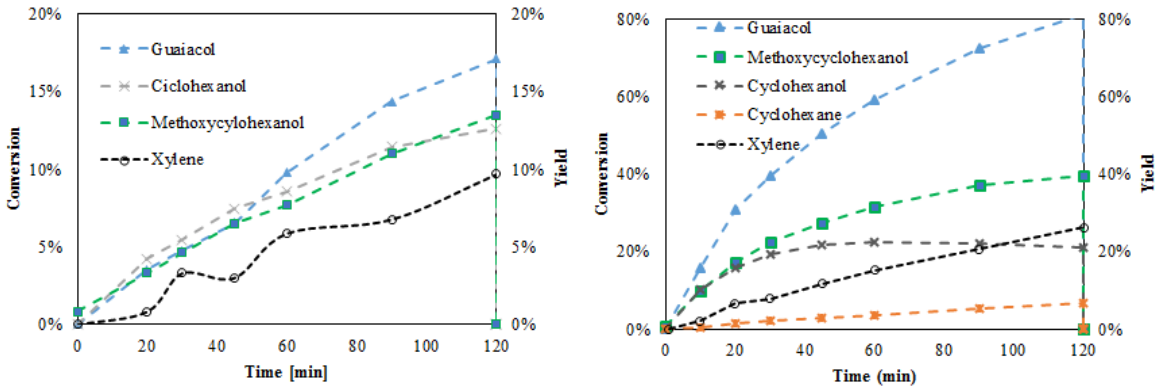
However, other authors have observed reactivity of acetic acid under other environments. Gutierrez-Rubito et al. [56] used ZSM-5 zeolite-supported nickel phosphide catalysts in the hydrotreating of guaiacol (3.3 wt %) and acetic acid (8 wt %) mixtures in decalin with temperatures between 260 and 300 ºC and 40 bar of hydrogen. They found a partial inhibition of guaiacol hydrodeoxygenation due to acetic acid competition for active sites. In the absence of hydrogen, they found that acetic acid-catalyzed and reacted with guaiacol to form guaiacol acetate via a reversible esterification route. Aliu et al. [57] analyzed the chemical kinetics of the HDO of vanillin and vanillin with acetic acid and found that the estimated activation energy was greater, approximately double, in the presence of acetic acid, evidencing the inhibition of the acid in the hydrodeoxygenation of vanillin.

2.2.4 Catalytic performance in the presence of water. Figure 6 shows the reactivity of guaiacol and xylene in presence of water at 190ºC and 250ºC. The products and therefore reaction route were similar to the ones found in the reference test (figure 3), only a slight decrease in the final conversion is observed,

[56] S. Gutiérrez-Rubio et al. ACS Omega. (2019) vol. 4, no. 25, pp. 21516–21528.
[57] E. Aliu, A. Hart, and J. Wood. Energy and Fuels. (2019) vol. 33, no. 11, pp. 11712–11723.

approximately a loss of 4 percentage points at 190ºC and 7 percentage points at 250ºC of the final conversion with respect to the reference test, which could be attributed to diffusion effects since in this test an emulsion was not made, and two phases were observed when loading the reactor for the tests. Furthermore, the conversion, yield, and reaction route was very similar to the case of the reference reaction without important changes in the catalytic behavior or in the textural properties of the material as shown previously in the hydrothermal treatment test. In this sense, all conversion and performance results of the water experiments are stored in the Annex B.

Figure 6. Reactivity results of guaiacol and xylene in presence of water at 190ºC (left) and 250ºC (right); pH2 = 69 bar; feed concentration: guaiacol 0.272 M and water 0.182 M in xylene.

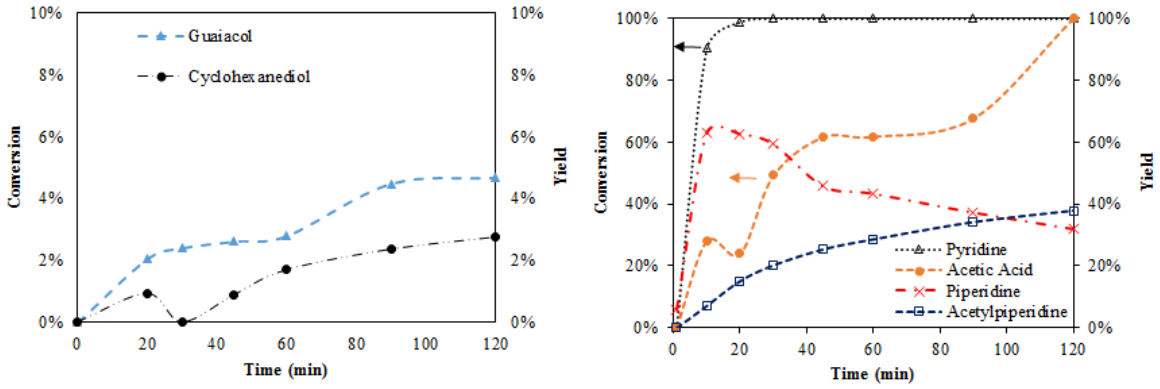


2.2.5 Catalytic performance in the presence of pyridine and acetic acid.

In this case, the catalyst was not active at 190°C as it occurred previously in the test made in the presence of pyridine. The results of the test at 250ºC are presented in figure 7. In this case, the conversion decreased below 5% and the only product detected was cyclohexanediol. On the other hand, pyridine rapidly converted to piperidine as it was the case when the test was done with the mixture of guaiacol and pyridine. According to results, piperidine further reacted with acetic acid to produce acetyl piperidine. On the other hand, xylene did not react. A blank test, i.e. without catalyst, was performed with the mixture of guaiacol, xylene, pyridine and

acetic acid and it was found that the mixture does not react in homogeneous phase (see results in Annex B).

Figure 7. Guaiacol reactivity in the presence of pyridine and acetic acid at 250ºC; pH_2 = 69 bar; feed concentration: guaiacol 0.272 M and pyridine 0.091 M and acetic acid 0.091 M in xylene (left). Conversion and yield of pyridine and acetic acid of the same test.



2.2.6 Catalytic performance in the presence of pyridine, acetic acid and water.

The other tests that were not presented due to similarity in the results can be consulted in Annex B, among them it is worth highlighting the test of reactivity of guaiacol with pyridine, acetic acid, and water is similar to the previous results of guaiacol in presence of pyridine and acetic acid, showing the same behavior in terms of: low rate of guaiacol conversion, the formation of cyclohexanediol without fully deoxygenated products, zero conversion of xylene, and the same reaction products for acetic acid and pyridine.

2.3 INFRARED SPECTROSCOPY ANALYSIS OF THE SPENT CATALYST.

Figure 8 shows ATR-infrared spectra for samples of the fresh catalyst and the spent catalyst from 3.2.1, 3.2.2 and 3.2.3 sections (3.2.1 section: guaiacol and xylene, 3.2.2 section: guaiacol, xylene and pyridine, and 3.2.3 section: guaiacol, xylene and acetic acid). The fresh catalyst only showed a peak at 1630 cm^{-1} associated to adsorbed water on material without previous degasification treatment [58]. In contrast, the catalyst spent in the reaction with guaiacol and xylene showed two new bands at 1493 cm^{-1} and 1452 cm^{-1}.The band at 1493 cm-1 attributed to vibrations of the resonance of the benzene ring of the guaiacol adsorbed on the support, due to an electron donation effect of guaiacol oxygen atoms on Lewis acid sites and the band at 1452 cm^{-1} attributed to guaiacol adsorbed by the methoxy group (OCH_3), inferring that under these conditions there is chemisorbed guaiacol doubly anchored by its oxygens, possibly forming methoxyphenate species on the catalyst support [47].

In the case of the catalyst spent in the test made in the presence of pyridine, it is observed that both materials have similar bands at 1500 cm^{-1}, with a small peak shift, and 1452 cm^{-1}, suggesting that both molecules interact with the catalyst in a similar way as described above. On the other hand, the peak at 1590 cm-1 is probably an indicative of a Lewis acid interaction with pyridine and Al^{VI} cation on γ-Al_2O_3 of the support that were used during the synthesis of the catalyst [43].

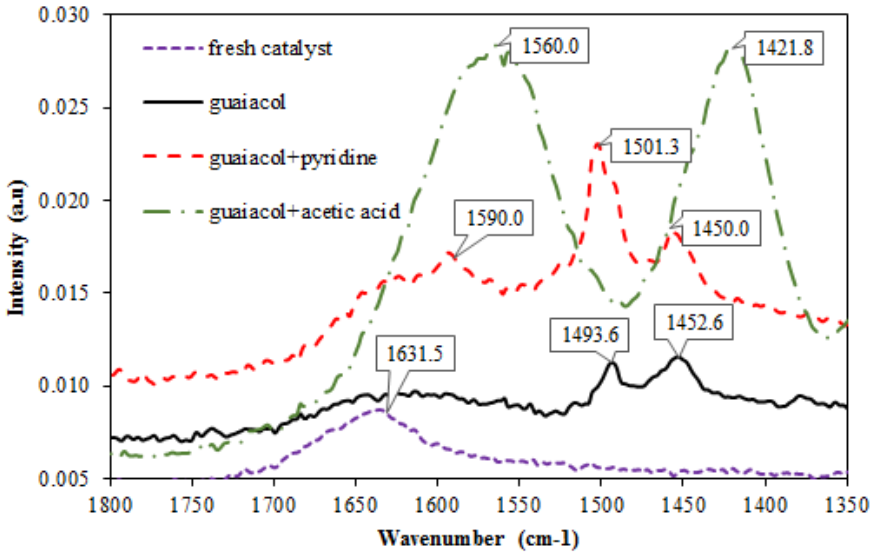
In the case of the catalyst spent in the test made in the presence of acetic acid, the ATR-IR spectrum showed bands at 1560 cm^{-1} and 1421 cm^{-1}, attributed to the possible formation of bidentate acetate. Hoffman et al. [59] studied the adsorption and reaction of acetic acid on nickel with different coatings using TPD and analysis

[43] M. A. Ardagh et al. ACS Catal. (2016) vol. 6, no. 9, pp. 6156–6164.
[47] X. Wang et al. Appl. Catal. A Gen. (2018) vol. 568, pp. 231–241.
[58] B. L. Mojet, S. D. Ebbesen, and L. Lefferts. Chem. Soc. Rev. (2010) vol. 39, no. 12, pp. 4643–4655.
[59] M. S. Hofman et al. Langmuir. (2020) vol. 36, no. 30, pp. 8705–8715.

of calculations by DFT and detected that at the beginning of the reaction the acid was chemically adsorbed on the surface of the nickel in low coatings, forming two bridges through the oxygens forming a species of bidentate acetate with a characteristic band at 1429 cm^{-1}, similar to obtained here at 1421cm^{-1} but when it exceeded 0.36 monolayers, the acid was in a condensed state, in which dimers and "cathemers" (chains of several acetic acid molecules group together to form multilayers). Upon reaching a temperature of 77ºC, it is observed that the acetate structures decompose into CO, and above 152 ºC only carbon remains on the surface, products that were not detected in this study.

In the case of water, the spectrum was similar to that of the reference test without new peaks and in the spectra of the other mixtures, a sum of the previously exposed peaks was observed according to each case.

Figure 8. Infrared spectrum of the catalyst fresh and after reaction at 250ºC and 69 bar of H2 pressure with guaiacol, guaiacol+pyridine, and guaiacol+acetic acid in xylene.



2.4 GLOBAL RESULTS OF CATALYTIC ACTIVITY AND YIELD TO ISO CONVERSION OF GUAIACOL.

Table 5 shows the catalytic activity data in terms of the apparent initial rate constant of consumption of guaiacol ($cm^3*min^{-1}*g_{cat}^{-1}$) and xylene. In general, it was observed that the reference reactions, without co-reactants, had a highest initial rate constant speed and then following the order of higher activity in presence of water>acetic acid>pyridine. Pyridine is seen to inhibit more strongly since the constants of the tests at 190 ºC with pyridine were all 0, while in the case of acid the speed is decreased but it is not deactivated at that temperature. For the hydrogenation of xylene lower initial rate constants were observed due to preferential guaiacol adsorption on catalyst surface but maintain the order of the activity in presence of the other co-reactants.

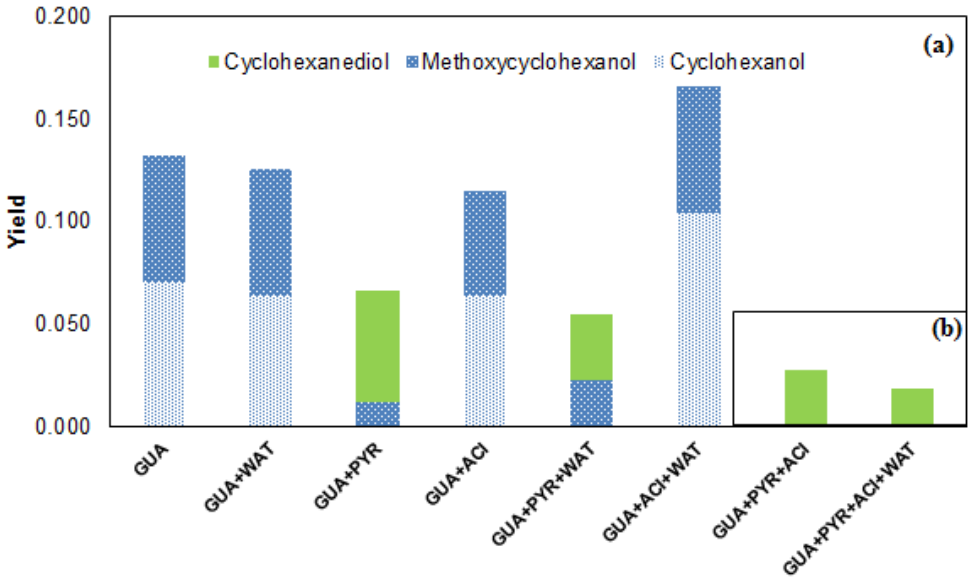
Table 5. Results of catalytic activity for all experiments.

Reaction mixture	k_{gua} ($min^{-1}g^{-1}cm^3$) at 190ºC	k_{gua} ($min^{-1}g^{-1}cm^3$) at 250ºC	k_{xyl} ($min^{-1}g^{-1}cm^3$) at 190ºC	k_{xyl} ($min^{-1}g^{-1}cm^3$) at 250ºC
guaiacol + xylene	0.754	8.296	0.279	1.829
guaiacol + xylene + water	0.721	7.99	0.184	1.523
guaiacol + xylene + pyridine	0	0.355	0	0
guaiacol + xylene + acetic acid	0.128	0.701	0	0.483
guaiacol + xylene + water + pyridine	0	0.762	0	0
guaiacol + xylene + pyridine + acetic acid	0	0.367	0	0
guaiacol + xylene + water + acetic acid	0.035	2.22	0	0.485
guaiacol + xylene+ water + pyridine + acetic acid	0	0.105	0	0

The iso-conversion performance data of the tests at 250ºC are presented in Figure 9, where considerable changes are found. In the reactions where both acid and pyridine are found in the same mixture (last two) it was found that the conversion is very low (5%) and they are analyzed separately. It is observed that in general methoxycylohexanol and cyclohexanol are always produced. However, introducing

pyridine affects the reaction pathway, producing a non-deoxygenated product, cyclohexanediol. This may be because pyridine and its products interacts with deoxygenation sites, modifying or inhibiting them in such a way that an alternate route is followed. These results suggest that for a process of hydrotreating bio-oils and even co-processing with hydrocarbons using this catalyst, it is necessary to remove nitrogenous compounds such as pyridine by means of a previous HDN unit, and organic acid compounds such as acetic acid using a process of esterification as a pre-treatment of the bio-oil.

Figure 9. Yields to iso-conversion of 10% guaiacol (a). Yields to iso-conversion of 5% guaiacol (b).



3. CONCLUSIONS

A global and systematic study of the Influence of the presence of representative molecules of pyrolysis bio-oils on the co-processing of guaiacol and xylene over a nickel/aluminosilicate catalyst was carried out, where the analysis of the physicochemical properties of the material, concentration of each of their compounds as a function of time and temperature allowed the following conclusions to be elucidated:

• Pyridine it is hydrogenated, affects activity and selectivity of guaiacol, attacks, and competes for metallic and acid sites of the support. Completely inhibits the hydrogenation of xylene. Its presence deactivates the catalyst completely at 190 °C.

• Acetic acid affects activity but not selectivity, occupies metallic sites, and allows the xylene to react. Both model molecules, guaiacol and the xylene, hydrogenate at a much slower rate and maintain the route of reference test. In the presence of pyridine it reacts to produce acetyl piperidine.

• Water under the conditions used does not substantially affect activity or selectivity of guaiacol.

BIBLIOGRAFY

ALIU, ELIAS, ABARASI HART, AND JOSEPH WOOD. Reaction Kinetics of Vanillin Hydrodeoxygenation in Acidic and Nonacidic Environments Using Bimetallic PdRh/Al2O3 Catalyst. *Energy and Fuels*. 2019. 33(11), pp. 11712–23.

ARDAGH, M. ALEXANDER, ZHENYU BO, SCOTT L. NAUERT, and Justin M. Notestein. Depositing SiO2 on Al2O3: A Route to Tunable Brønsted Acid Catalysts. *ACS Catalysis*. 2016. 6(9), pp. 6156–64.

ARDIYANTI, A. R. et al. Ni-Based Catalysts for the Hydrotreatment of Fast Pyrolysis Oil. *Energy and Fuels.* 2016. 30(3), pp. 1544–54.

ARTUNDUAGA, SERGIO, AND CAMILO PERALTA. Análisis Cinético Del Comportamiento de Un Catalizador Basado En Níquel y Aluminosilicato En La Hidrodesoxigenación de Guayacol. Trabajo de Grado Ingeniería Química. Universidad Industrial de Santander. 2020.

BARRETT, ELLIOTT P., LESLIE G. JOYNER, AND PAUL P. HALENDA. The Determination of Pore Volume and Area Distributions in Porous Substances. I. Computations from Nitrogen Isotherms. *Journal of the American Chemical Society*. 1951. 73(1), pp. 373–80.

BEZERGIANNI, STELLA, ATHANASSIOS DIMITRIADIS, OLEG KIKHTYANIN, and DAVID KUBICKA. Refinery Co-Processing of Renewable Feeds. *Progress in Energy and Combustion Science.* 2018. 68, pp. 29–64.

BROGLIA, FRANCESCA et al. Guaiacol Hydrodeoxygenation as a Model for Lignin Upgrading. Role of the Support Surface Features on Ni-Based Alumina-Silica Catalysts. *Fuel*. 2019. 243(January 2018), pp. 501–8.

BRUNAUER, STEPHEN, P. H. EMMETT, AND EDWARD TELLER. Adsorption of Gases in Multimolecular Layers*. Journal of the American Chemical Society*. 1938. 60(2), pp. 309–19.

BUI, VAN NGOC, DOROTHÉE LAURENTI, PAVEL AFANASIEV, AND CHRISTOPHE GEANTET. Hydrodeoxygenation of Guaiacol with CoMo Catalysts. Part I: Promoting Effect of Cobalt on HDO Selectivity and Activity. *Applied Catalysis B: Environmental*. 2011. 101(3–4), pp. 239–45.

BYKOVA, M. V. et al. Stabilized Ni-Based Catalysts for Bio-Oil Hydrotreatment: Reactivity Studies Using Guaiacol. *Catalysis Today.* 2014. 220–222, pp. 21–31.

BYKOVA, M. V., S. G. ZAVARUKHIN, L. I. TRUSOV, AND V. A. YAKOVLEV. Guaiacol Hydrodeoxygenation Kinetics with Catalyst Deactivation Taken into Consideration. *Kinetics and Catalysis.* 2013. 54(1), pp. 40–48.

CELIS-CORNEJO, CARLOS M., DAVID J. PÉREZ-MARTÍNEZ, JORGE A. ORREGO-RUIZ, AND VÍCTOR G. BALDOVINO-MEDRANO. Identification of Refractory Weakly Basic Nitrogen Compounds in a Deeply Hydrotreated Vacuum Gas Oil and Assessment of the Effect of Some Representative Species over the Performance of a Ni-MoS2/Y-Zeolite-Alumina Catalyst in Phenanthrene Hydrocracking. *Energy and Fuels*. 2018. 32(8), pp. 8715–26.

CHENG, TINGTING, YEHUA HAN, YANFEN ZHANG, AND CHUNMING XU. Molecular Composition of Oxygenated Compounds in Fast Pyrolysis Bio-Oil and Its Supercritical Fluid Extracts. *Fuel*. 2016. 172, pp. 49–57.

CHUKWUNEKE, J. L., M. C. EWULONU, I. C. CHUKWUJIKE, AND P. C. OKOLIE. Physico-Chemical Analysis of Pyrolyzed Bio-Oil from Swietenia Macrophylla (Mahogany) Wood. *Heliyon*. 2019. 5(6), pp. 1–7.

EL-KEMARY, M., N. NAGY, AND I. EL-MEHASSEB. Nickel Oxide Nanoparticles: Synthesis and Spectral Studies of Interactions with Glucose. *Materials Science in Semiconductor Processing.* 2013. 16(6), pp. 1747–52.

ELLIOTT, D C, AND E G BAKER. Catalytic Hydrotreating of Biomass Liquefaction Products to Produce Hydrocarbon Fuels: Interim Report. *United States. Dept. of Energy. Office of Scientific and Technical Information.* 1986. (1), pp. 1–64.

EMEIS, C. A. Determination of Integrated Molar Extinction Coefficients for Infrared Absorption Bands of Pyridine Adsorbed on Solid Acid Catalysts. *Journal of Catalysis*. 1993. 141(2), pp. 347–54.

ESPINOZA PÉREZ, ANDREA TERESA, MAURICIO CAMARGO, PAULO CÉSAR NARVÁEZ RINCÓN, AND MIGUEL ALFARO MARCHANT. Key Challenges and Requirements for Sustainable and Industrialized Biorefinery Supply Chain Design and Management: A Bibliographic Analysis. *Renewable and Sustainable Energy Reviews.* 2017. 69(October 2016), pp. 350–59.

EVANS, ROBERT J, AND THOMAS A MILNE. Molecular Characterization of Pyrolysis of Biomass. 1. Fundamentals. *Energy & Fuels*. 1987. 1(2), pp. 123–38.

FARRAUTO, ROBERT J, AND MELVIN C HOBSON. Catalyst Characterization. In ed. *Robert A B T - Encyclopedia of Physical Science and Technology (Third Edition) Meyers*. New York: Academic Press, 501–26.

GEVERT, B S, J-E. OTTERSTEDT, AND F E MASSOTH. Kinetics of the HDO of Methyl-Substituted Phenols. *Applied Catalysis*. 1987. 31(1), pp. 119–31.

GONZÁLEZ-BORJA, MIGUEL ÁNGEL, AND DANIEL E. RESASCO. Anisole and Guaiacol Hydrodeoxygenation over Monolithic Pt-Sn Catalysts. *Energy and Fuels.* 2011. 25(9), pp. 4155–62.

GOULAS, KONSTANTINOS A. et al. Fundamentals of C–O Bond Activation on Metal Oxide Catalysts. *Nature Catalysis*. 2019. 2(3), pp. 269–76.

GUTIÉRREZ-RUBIO, SANTIAGO, INÉS MORENO, DAVID P. SERRANO, AND JUAN M. CORONADO. Hydrotreating of Guaiacol and Acetic Acid Blends over Ni2P/ZSM-5 Catalysts: Elucidating Molecular Interactions during Bio-Oil Upgrading. *ACS Omega*. 2019. 4(25), pp. 21516–28.

GUTIERREZ, ANDREA, EEVA MAIJA TURPEINEN, TUULA RIITTA VILJAVA, AND OUTI KRAUSE. Hydrodeoxygenation of Model Compounds on Sulfided CoMo/G-Al2O3 and NiMo/G-Al2O3 Catalysts; Role of Sulfur-Containing Groups in Reaction Networks*. Catalysis Today.* 2017. 285, pp. 125–34.

HELLINGER, MELANIE et al. Catalytic Hydrodeoxygenation of Guaiacol over Platinum Supported on Metal Oxides and Zeolites. *Applied Catalysis A: General.* 2015. 490, pp. 181–92.

HENSLEY, ALYSSA J.R., YONG WANG, DONGHAI MEI, AND JEAN SABIN MCEWEN. Mechanistic Effects of Water on the Fe-Catalyzed Hydrodeoxygenation of Phenol. the Role of Brønsted Acid Sites*. ACS Catalysis*. 2018. 8(3), pp. 2200–2208.

HOFMAN, MICHELLE S. et al. Acetic Acid Adsorption and Reactions on Ni(110). *Langmuir*. 2020. 36(30), pp. 8705–15.

HONG, YOON KI, DAE WON LEE, HEE JUN EOM, AND KWAN YOUNG LEE. The Catalytic Activity of Pd/WOx/?-Al2O3 for Hydrodeoxygenation of Guaiacol. *Applied Catalysis B: Environmental.* 2014. 150–151, pp. 438–45.

JAHROMI, HOSSEIN, AND FOSTER A. AGBLEVOR. Hydrotreating of Guaiacol: A Comparative Study of Red Mud-Supported Nickel and Commercial Ni/SiO2-Al2O3 Catalysts. *Applied Catalysis A: General.* 2018. 558, pp. 109–21.

KAY LUP, ANDREW NG, FAISAL ABNISA, WAN MOHD ASHRI WAN DAUD, AND MOHAMED KHEIREDDINE AROUA. A Review on Reactivity and Stability of Heterogeneous Metal Catalysts for Deoxygenation of Bio-Oil Model Compounds. *Journal of Industrial and Engineering Chemistry.* 2017. 56, pp. 1–34.

Laurent, E., A. Centeno, and B. Delmon. Coke Formation during the Hydrotreating of Biomass Pyrolysis Oils: Influence of Guaiacol Type Compounds. *Studies in Surface Science and Catalysis.* 1994. 88(C), pp. 573–78.

LAURENT, ETIENNE, AND BERNARD DELMON. Study of the Hydrodeoxygenation of Carbonyl, Carboxylic and Guaiacyl Groups over Sulfided CoMo/?-Al2O3 and NiMo/?-Al2O3 Catalyst. I. Catalytic Reaction Schemes*. Applied Catalysis A, General.* 1994. 109(1), pp. 77–96.

LEIVA, K. et al. Kinetic Study of the Conversion of 2-Methoxyphenol over Supported Re Catalysts: Sulfide and Oxide State. *Applied Catalysis A: General.* 2015. 505, pp. 302–8.

LI, CONGCONG et al. Hydrodeoxygenation of Guaiacol to Phenol over Ceria-Supported Iron Catalysts. *ACS Catalysis.* 2020., pp. 14624–39.

LIU, YANG et al. Characterization of Red Pine Pyrolysis Bio-Oil by Gas Chromatography-Mass Spectrometry and Negative-Ion Electrospray Ionization Fourier Transform Ion Cyclotron Resonance Mass Spectrometry*. Energy and Fuels*. 2012. 26(7), pp. 4532–39.

LU, MOHONG et al. Hydrodeoxygenation of Guaiacol Catalyzed by High-Loading Ni Catalysts Supported on SiO2-TiO2 Binary Oxides. *Industrial and Engineering Chemistry Research*. 2019. 58(4), pp. 1513–24.

LYLYKANGAS, MIKKO S., PETRI A. RAUTANEN, AND A. OUTI I. KRAUSE. Liquid-Phase Hydrogenation Kinetics of Multicomponent Aromatic Mixtures on Ni/Al2O3. *Industrial and Engineering Chemistry Research*. 2002. 41(23), pp. 5632–39.

MOCHIZUKI, TAKEHISA, SHIH YUAN CHEN, MAKOTO TOBA, AND YUJI YOSHIMURA. Deoxygenation of Guaiacol and Woody Tar over Reduced Catalysts. *Applied Catalysis B: Environmental.* 2014. 146, pp. 237–43.

MOJET, BARBARA LOUISE, SUNE DALGAARD EBBESEN, AND LEON LEFFERTS. Light at the Interface: The Potential of Attenuated Total Reflection Infrared Spectroscopy for Understanding Heterogeneous Catalysis in Water. *Chemical Society Reviews.* 2010. 39(12), pp. 4643–55.

MOLINA, DIEGO, AND PAOLA SUÁREZ. Análisis de La Hidrodesoxigenación de Guayacol Bajo Diferentes Condiciones de Temperatura y Cantidad de Sitios Activos Sobre Un Catalizador de Níquel Soportado En Alúmina Modificada Con Silicio. Trabajo de Grado Ingeniería Química. Universidad Industrial de Santander. 2018.

MORA-VERGARA, IVÁN D. et al. Hydrodeoxygenation of Guaiacol Using NiMo and CoMo Catalysts Supported on Alumina Modified with Potassium. *Catalysis Today.* 2018. 302, pp. 125–35.

MORA, IVÁN D., EDNA MÉNDEZ, LISETH J. DUARTE, AND SONIA A. GIRALDO. Effect of Support Modifications for CoMo/?-Al2O 3 and CoMo/ASA Catalysts in the

Hydrodeoxygenation of Guaiacol. *Applied Catalysis A: General.* 2014. 474, pp. 59–68.

MU, WEI et al. Noble Metal Catalyzed Aqueous Phase Hydrogenation and Hydrodeoxygenation of Lignin-Derived Pyrolysis Oil and Related Model Compounds. *Bioresource Technology.* 2014. 173, pp. 6–10.

POPOV, ANDREY et al. Bio-Oils Hydrodeoxygenation: Adsorption of Phenolic Molecules on Oxidic Catalyst Supports. *Journal of Physical Chemistry C.* 2010. 114(37), pp. 15661–70.

RAVENELLE, RYAN M. et al. Structural Changes of ?-Al2O3-Supported Catalysts in Hot Liquid Water. *ACS Catalysis.* 2011. 1(5), pp. 552–61.

REDONDO, RAUL. Síntesis de Catalizadores NiCu Para Hdo de Guayacol Usando Como Soporte Alúmina y Alúmina Modificada Con Óxido de Silicio. Trabajo de Grado Ingeniería Química. Universidad Industrial de Santander. 2017.

RESTREPO-GARCIA, JONATAN R., GUSTAVO E. RAMÍREZ, AND VÍCTOR G. BALDOVINO-MEDRANO. Hydroprocessing of Phenanthrene Over Sulfided Fe–W Supported on Modified SBA-15. *Catalysis Letters*. 2018. 148(2), pp. 621–41.

RESTREPO, L., AND Y. PORTILLA. Optimización de Los Contenidos de Níquel y Silicio En El Catalizador Ni/Al2O3-Si Para Hidrodesoxigenación de Guayacol. Trabajo de Grado Ingeniería Química. Universidad Industrial de Santander. 2019.

ROBINSON, ALLISON M., JESSE E. HENSLEY, AND J. WILL MEDLIN. Bifunctional Catalysts for Upgrading of Biomass-Derived Oxygenates: A Review. *ACS Catalysis.* 2016. 6(8), pp. 5026–43.

RODRÍGUEZ-REINOSO, FRANCISCO. Characterization of Porous Solids VI: Preface. *Studies in Surface Science and Catalysis.* 2002. 144, pp. 49–56.

RYCZKOWSKI, JANUSZ. IR Spectroscopy in Catalysis. *Catalysis Today.* 2001. 68(4), pp. 263–381.

SONG, WENJI et al. Synergistic Effects of Ni and Acid Sites for Hydrogenation and C-O Bond Cleavage of Substituted Phenols. *Green Chemistry.* 2015. 17(2), pp. 1204–18.

THYBAUT, JORIS W., MARK SAEYS, AND GUY B. MARIN. Hydrogenation Kinetics of Toluene on Pt/ZSM-22. *Chemical Engineering Journal.* 2002. 90(1–2), pp. 117–29.

UDDIN, ABM HELAL et al. Comparative Study of Three Digestion Methods for Elemental Analysis in Traditional Medicine Products Using Atomic Absorption Spectrometry. *Journal of Analytical Science and Technology*. 2016. 7(1), pp. 1–7.

WANG, HUAMIN, JONATHAN MALE, AND YONG WANG. Recent Advances in Hydrotreating of Pyrolysis Bio-Oil and Its Oxygen-Containing Model Compounds. *ACS Catalysis.* 2013. 3(5), pp. 1047–70.

WANG, XUN et al. Ni Nanoparticles Entrapped in Nickel Phyllosilicate for Selective Hydrogenation of Guaiacol to 2-Methoxycyclohexanol. *Applied Catalysis A: General.* 2018. 568, pp. 231–41.

ZHAO, JIE, HUI CHEN, JUN XU, AND JIANYI SHEN. Effect of Surface Acidic and Basic Properties of the Supported Nickel Catalysts on the Hydrogenation of Pyridine to Piperidine. *Journal of Physical Chemistry C.* 2013. 117(20), pp. 10573–80.

ZHENG, ANQING et al. Controlling Deoxygenation Pathways in Catalytic Fast Pyrolysis of Biomass and Its Components by Using Metal-Oxide Nanocomposites. *iScience*. 2020. 23(1), pp. 1–14.

ANNEXES

ANNEX A. Preliminary tests (Pretests).

Table A1. Results of all preliminary tests. Weight percent in the reaction mixture (wt%) and conversion percent (X) after 1 hour with 0.15 g of Ni/Aluminosilicate catalyst. Reaction at 250ºC and pH2 = 6.9 MPa.

Compound	Pretest 1		Pretest 2		Pretest 3		Pretest 4		Pretest 5		Pretest 6	
	wt%	X	wt%	X	wt%	X	wt%	X	wt%	X	wt%	X
Guaiacol	3.70%	8.20%	22.20%	0.00%	3.70%	9.40%	3.70%	9.42%	3.70%	0.00%	3.70%	0.00%
Water	3.00%	0.00%	6.00%	0.00%	0.00%	0.00%	0.00%	0.00%	1.50%	0.00%	0.12%	0.00%
Pyridine	0.00%	0.00%	0.50%	0.00%	0.00%	0.00%	0.08%	100.00%	0.13%	86.53%	0.50%	81.00%
Acetic acid	0.00%	0.00%	10.00%	0.00%	10.00%	0.00%	0.00%	0.00%	2.50%	0.00%	0.40%	0.00%
Xylene	91.30%	3.00%	59.30%	0.00%	84.30%	0.00%	94.25%	0.00%	90.20%	0.55%	57.50%	0.00%
Dodecane	2.00%	0.00%	2.00%	0.00%	2.00%	0.00%	2.00%	0.00%	2.00%	0.00%	1.25%	0.00%

ANNEX B. Results of evolution of conversion and performance of Guayacol of all the tests of the model carried out.

The following tests presented zero guaiacol conversion:

- Test with guaiacol and pyridine at 190ºC.
- Test with guaiacol, pyridine and acetic acid at 190ºC.
- Test with guaiacol, pyridine and water at 190ºC.
- Test with guaiacol, acetic acid, pyridine and water at 190ºC.

Figure B1. Conversion and yield results of test with guaiacol, acetic acid and water at 190ºC

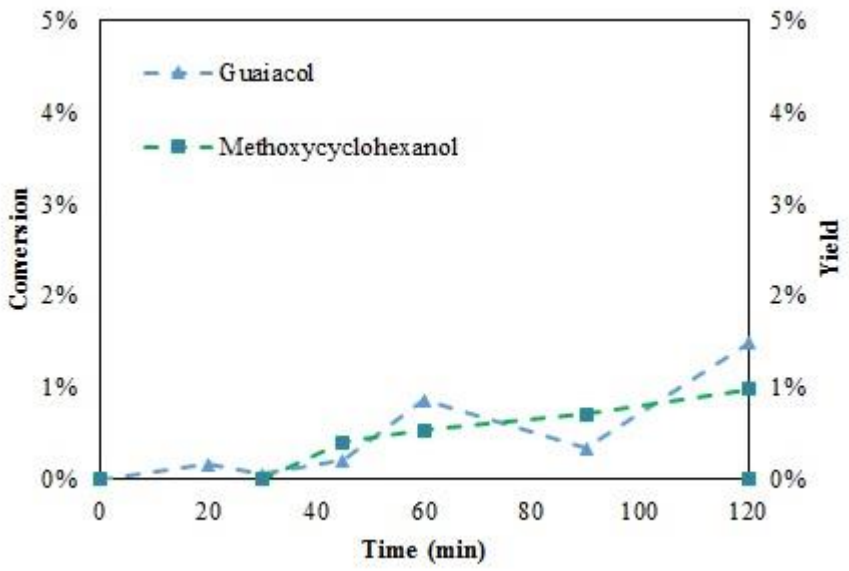


Figure B2. Conversion and yield results of test with guaiacol, pyridine and water at 190ºC.

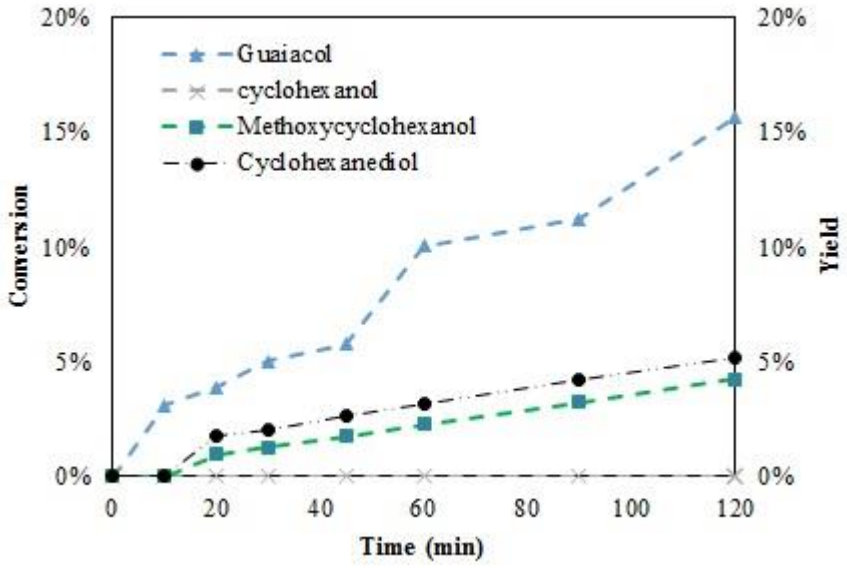


Figure B3. Conversion and yield results of test with guaiacol, acetic acid and water at 250ºC**.**

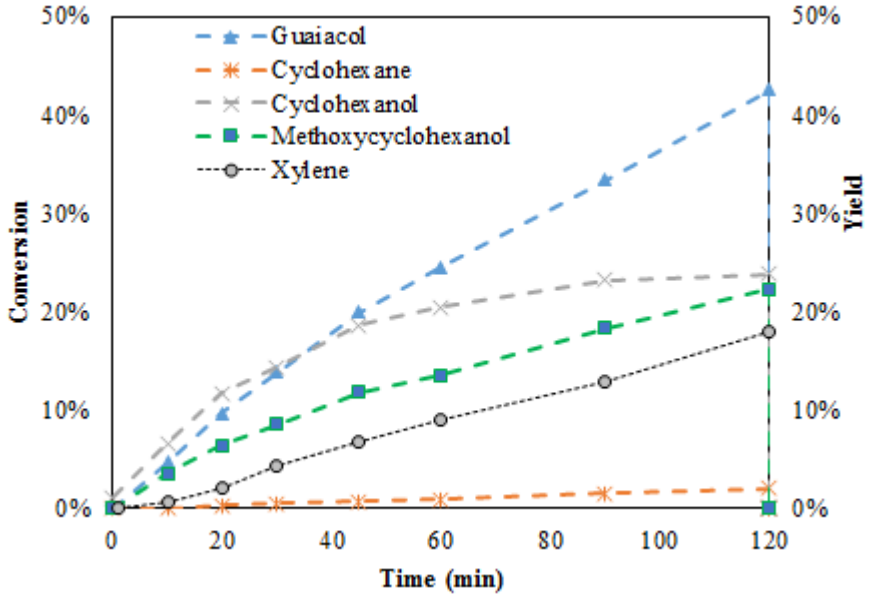
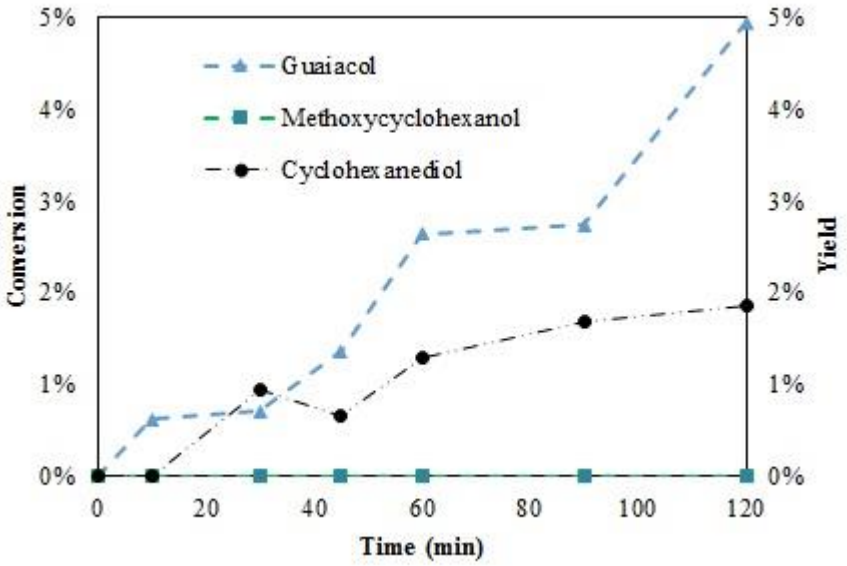


Figure B4. Conversion and yield results of test with guaiacol, acetic acid, pyridine and water at 250ºC



ANNEX C. Results of physicochemical properties.

Figure C1. FT-IR spectrum of the aluminosilicate support after pyridine desorption at 150ºC.

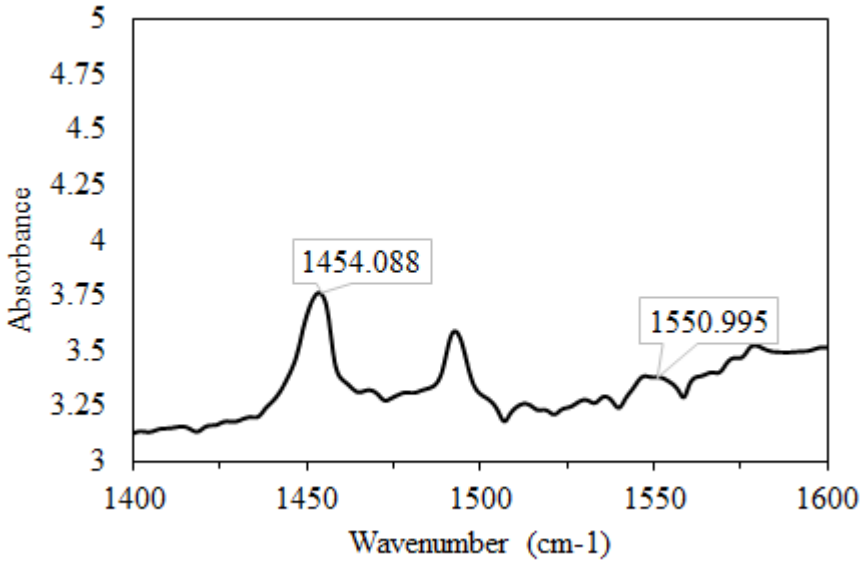


Figure C2. Isotherms of the alumina material before (Al) and after the hydrothermal test (Al-HT).

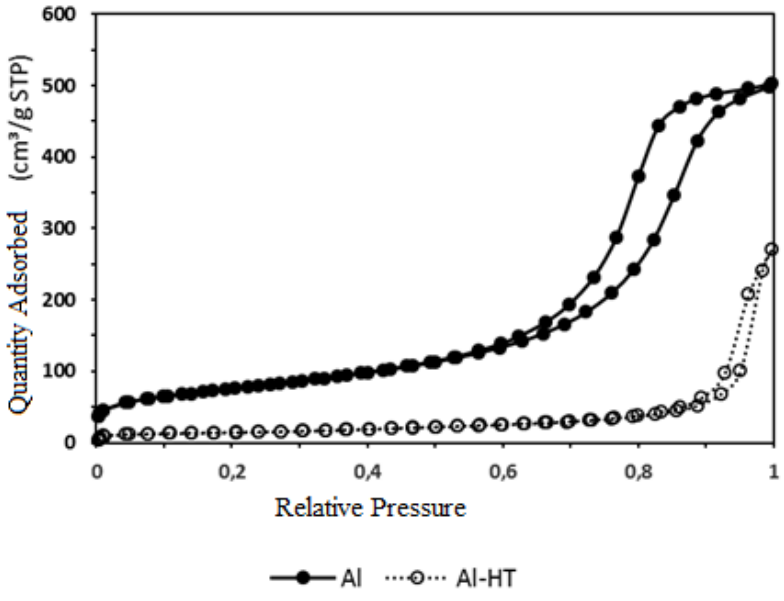


Figure C3. Isotherms of the nickel catalyst supported in alumina chemically modified with silicon before (NiAlSi) and after the hydrothermal test (NiAlSi-HT).

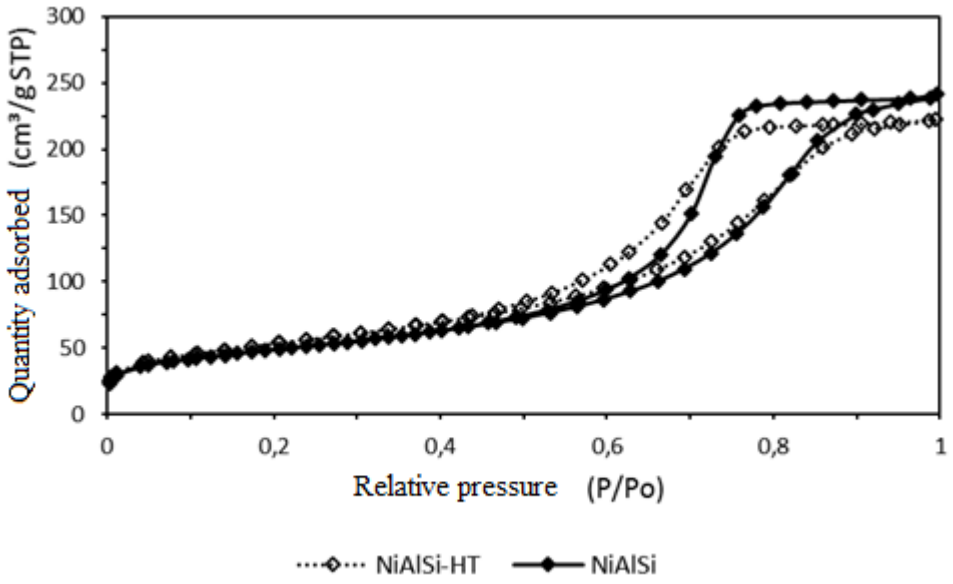
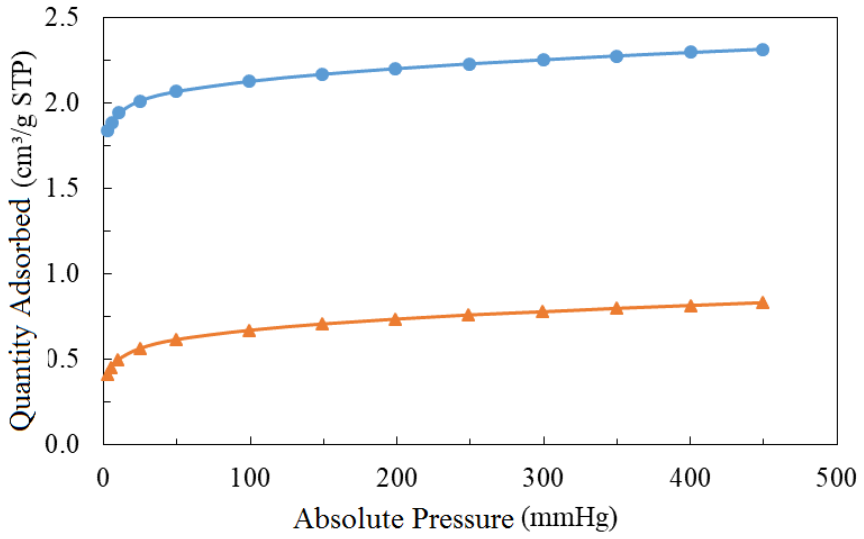
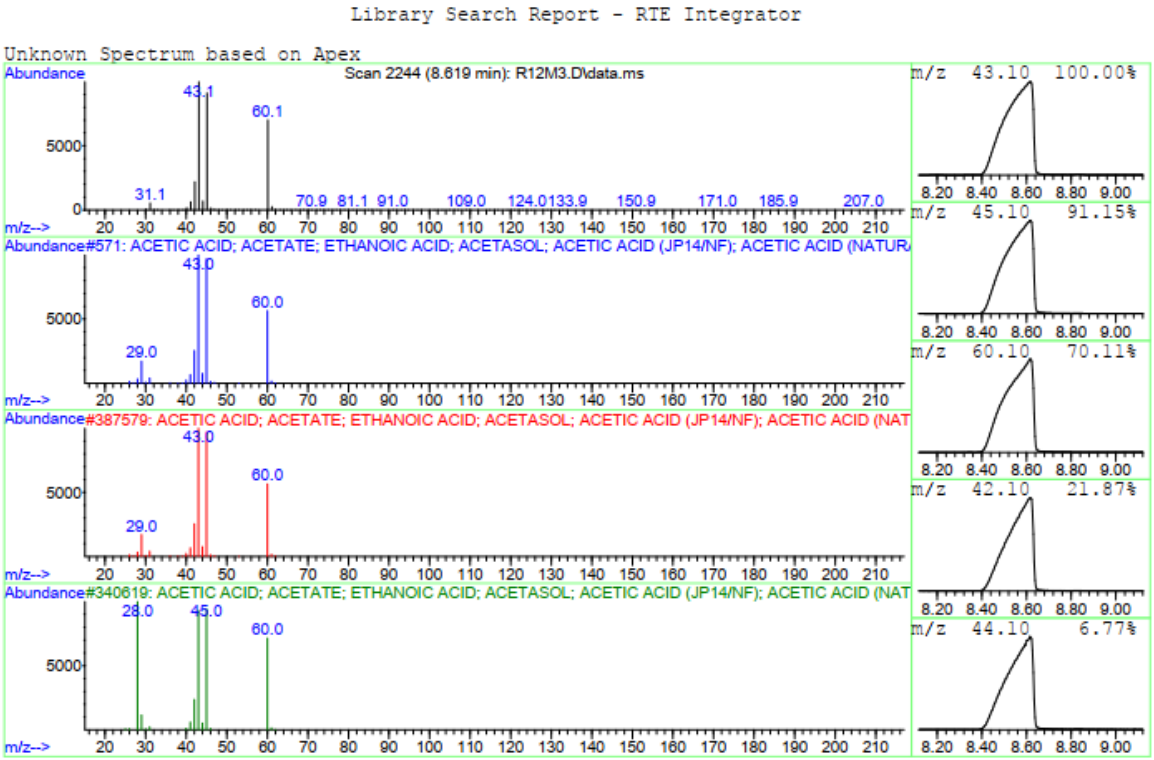


Figure C4. Static volumetric chemisorption isotherms of H2 at 35 ° C.



ANNEX D. Mass spectrum of Acetic Acid and Dioxane in preliminary test 2.

Figure D1. Mass Spectrum of Acetic Acid in preliminary test vial 2.

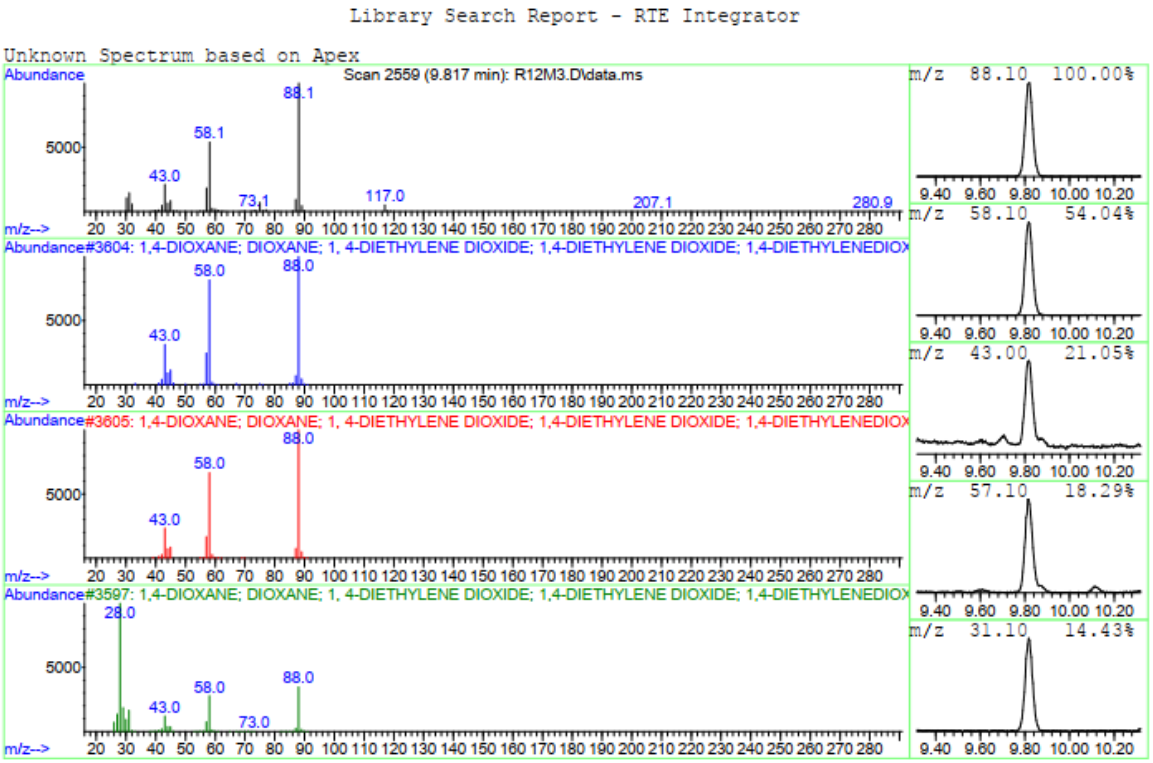


Data File: C:\msdchem\CORRIDAS\2019\CICTA\R12M3.D
Sample :

Peak Number: 2 at 8.619 min Area: 166710013 Area % 7.03

The 3 best hits from each library.	Ref\#	CAS\#	Qual
D:\DATABASE\W8.1			
1 ACETIC ACID; ACETATE; ETHANOIC A...	571	000064-19-7	91
2 ACETIC ACID; ACETATE; ETHANOIC A...	387579	000064-19-7	91
3 ACETIC ACID; ACETATE; ETHANOIC A...	340619	000064-19-7	91
C:\Database\AMHS_1.L	No hits were retrieved.		

Figure D2. Mass Spectrum of Dioxane in preliminary test vial 2.



Data File: C:\msdchem\CORRIDAS\2019\CICTA\R12M3.D
Sample :

Peak Number: 3 at 9.817 min Area: 908176 Area % 0.04

The 3 best hits from each library.	Ref\#	CAS\#	Qual
D:\DATABASE\W8.1			
1 1,4-DIOXANE; DIOXANE; 1, 4-DIETH...	3604	000123-91-1	86
2 1,4-DIOXANE; DIOXANE; 1, 4-DIETH...	3605	000123-91-1	80
3 1,4-DIOXANE; DIOXANE; 1, 4-DIETH...	3597	000123-91-1	78
C:\Database\AMHS_1.L	No hits were retrieved.		